Molecular Therapy
Methods & Clinical Development
Original Article

Extracellular vesicle depletion and UGCG overexpression mitigate the cell density effect in HEK293 cell culture transfection

Pol Pérez-Rubio,[1,3] Jesús Lavado-García,[1,2,3] Laia Bosch-Molist,[1] Elianet Lorenzo Romero,[1] Laura Cervera,[1] and Francesc Gòdia[1]

[1]Grup d'Enginyeria de Bioprocessos i Biocatàlisi Aplicada, Escola d'Enginyeria, Universitat Autònoma de Barcelona, Campus de Bellaterra, Cerdanyola del Vallès, 08193 Barcelona, Spain

The hitherto unexplained reduction of cell-specific productivity in transient gene expression (TGE) at high cell density (HCD) is known as the cell density effect (CDE). It currently represents a major challenge in TGE-based bioprocess intensification. This phenomenon has been largely reported, but the molecular principles governing it are still unclear. The CDE is currently understood to be caused by the combination of an unknown inhibitory compound in the extracellular medium and an uncharacterized cellular change at HCD. This study investigates the role of extracellular vesicles (EVs) as extracellular inhibitors for transfection through the production of HIV-1 Gag virus-like particles (VLPs) via transient transfection in HEK293 cells. EV depletion from the extracellular medium restored transfection efficiency in conditions that suffer from the CDE, also enhancing VLP budding and improving production by 60%. Moreover, an alteration in endosomal formation was observed at HCD, sequestering polyplexes and preventing transfection. Overexpression of UDP-glucose ceramide glucosyltransferase (UGCG) enzyme removed intracellular polyplex sequestration, improving transfection efficiency. Combining EV depletion and UGCG overexpression improved transfection efficiency by ∼45% at 12 × 10^6 cells/mL. These results suggest that the interaction between polyplexes and extracellular and intracellular vesicles plays a crucial role in the CDE, providing insights for the development of strategies to mitigate its impact.

INTRODUCTION

The biopharmaceutical industry is moving toward tailor-made and precision therapies that require adaptive bioprocesses. In addition, in response to the emergence of new viral outbreaks, efforts are being made to improve the versatility and responsiveness of biologics manufacturing.[1,2] Transient gene expression (TGE) technology stands out as an attractive strategy that may help approach these questions. Using TGE, production titers can reach the range of g/L in a time span of weeks,[3,4] eliminating the high time-demanding tasks of clonal selection and characterization required for stable gene expression (SGE).[5] Since the production of a completely different biopharmaceutical only requires the use of different plasmids, TGE offers the flexibility of producing a wide range of biologics without the need to readapt the bioprocessing equipment.[6–8] Nevertheless, SGE is still the leading methodology at industrial-scale biomanufacturing in most animal cell-based bioprocesses, while TGE is usually employed in R&D and preclinical stages.[9] However, some commercial bioprocesses still require TGE at both lab and industrial scale, such as the production of recombinant adeno-associated virus (rAAV).[10,11]

Despite the benefits of TGE, large-scale processes cannot be successfully scaled-up since a major drawback restricts production at high cell densities (HCDs), known as the cell density effect (CDE).[12,13] This phenomenon is regarded as a reduction in cell-specific productivity when cultures are transfected at densities above their mid-exponential phase.[14,15] The CDE does not exclusively affect mammalian cells but also extends to transfection of insect cells and infection processes, being also described in insect and avian cells when working with baculovirus and viral infections.[16–20] The limiting cell density varies depending on the cell line, operation mode, and production strategy, but it consistently leads to a reduction in specific productivity, resulting in suboptimal volumetric productivity states.[20–26] Understanding the physiological causes of the CDE and allowing successful transfection at higher densities would increase the commercial exploitation of many TGE-based biologics, as their large-scale production processes are currently unfeasible. Higher titers would also contribute to a reduction of manufacturing costs, counteracting the cost of large amounts of GMP-grade plasmid required for TGE.[7]

Received 1 September 2023; accepted 12 January 2024;
https://doi.org/10.1016/j.omtm.2024.101190.

[2]Present address: Novo Nordisk Foundation Center for Biosustainability, Technical University of Denmark, 2800 Kgs. Lyngby, Denmark

[3]These authors contributed equally

Correspondence: Pol Pérez-Rubio, Grup d'Enginyeria de Bioprocessos i Biocatàlisi Aplicada, Escola d'Enginyeria, Universitat Autònoma de Barcelona, Campus de Bellaterra, Cerdanyola del Vallès, 08193 Barcelona, Spain.
E-mail: pol.perez@uab.cat

Previous research on the CDE showed that it can be explained as a combination of two independent factors. First, an unknown extracellular inhibitory compound.

Incorporating continuous medium replacement (MR) steps has been reported to improve transfection efficiency by removing conditioned spent medium, which is hypothesized to eliminate potential inhibitors.[21,22] Secondly, an alteration in cell physiology triggered at HCD, as concentrating cells from low to high density is enough to observe the CDE.[23] Recently, state-of-the-art multiplexed proteomic analyses also unveiled limitations in lipid biosynthesis and cargo transport at HCD.[24] Interestingly, previous studies also showed that biosynthetic and transport pathways for naturally occurring extracellular vesicles (EVs) were also upregulated.[25]

In this work, EVs have been studied as the potential key player leading to the CDE at HCD, explaining both the extracellular inhibition and the intracellular trafficking alteration. EVs are membrane-derived nanostructures that are constitutively produced by the cell.[26,27] These heterogeneous populations of vesicles are fundamental for cell-to-cell communication in a wide range of biological processes.[28] They mediate in organ development,[29] neural communication,[30] cell migration,[31] inflammatory responses,[32] remodeling of the extracellular matrix,[33,34] and even may play a role in the pathogenesis of many diseases.[35–37] Moreover, numerous EV transmembrane proteins, such as integrins and tetraspanins, are reported to be involved in interactions with the extracellular matrix and surrounding molecules.[38] Despite their increasing influence on the biomedicine and biotechnology fields, many of the potential implications of EVs are still undefined. Internalization pathways upon EV uptake depend on the recipient cell line, yet this can occur through dynamin polymerization and receptor-mediated endocytosis.[38] Moreover, EV clusters or aggregates enter cells through direct phagocytosis.[39] Interestingly, polyethylenimine:DNA (PEI:DNA) polyplex uptake happens upon flotillin or dynamin polymerization prior to an interaction with membrane proteoglycans.[40] Given that EVs are glycosylated structures, they may potentially interfere with the transfection process, thereby hindering both extra- and intracellular non-viral gene delivery. Thus, EV metabolism might integrate the two components comprising the CDE being able to provide an alternative explanation to the molecular causes underlying this issue. Here, we present a rational investigation to address the CDE observed in HEK293 cells upon production of HIV-1 Gag virus-like particles (VLPs) by TGE. The transfection process was characterized at increasing cell densities to assess the nature of the problem. Insights into the influence of cell culture medium and intracellular interactions were gained by coupling quantification using nanoparticle tracking analysis (NTA) and intracellular tracking. Also, the findings resulting from the studies on transient transfection were applied in infection processes based on adenoviruses (AdVs) to find common features between the CDE observed in infection and transfection. Altogether this research contributes to understand the CDE and paves the way to further solve it and broaden the scope of bioprocess engineering and its applicability.

RESULTS

Cell-specific productivity in TGE decreases when concentrating metabolically active cells to HCD

The production of HIV-1 Gag polyprotein fused to eGFP (Gag::eGFP) upon TGE was used to test transfection efficiency at different cell densities. With no MR step, cells were grown in parallel and transfected at increasing densities from 2 to 12 $\times$ 10^6 cells/mL. Transfection was carried out when the cell culture achieved the targeted cell density with no concentration step. A drastic reduction in transfection efficiency can be observed as cell density increased (Figure 1A). This was translated in a parallel reduction in HIV-1 Gag VLP-specific productivity, completely preventing VLP production if transfection was carried out at cell densities higher than 6 $\times$ 10^6 cells/mL (Figure 1B). In these transfections, the number of plasmid copies coding for Gag::eGFP delivered ranged from 7.27 $\times$ 10^4 copies/cell when transfecting at 2 $\times$ 10^6 cells/mL down to 1.21 $\times$ 10^4 copies/cell when transfecting at 12 $\times$ 10^6 cells/mL. To verify that the observed reduction in transfection efficiency was not due to a lack of Gag::eGFP-coding DNA, transfections using low pGag::eGFP copy number were carried out at 2 $\times$ 10^6 cells/mL. In all transfections, the total amount of DNA remained constant but pGag::eGFP copies decreased as the amount of stuffer DNA increased. This confirmed that, at all studied cell densities, the number of pGag::eGFP copies used was enough to sustain transfection (Figure 1C). When transfecting at 8 $\times$ 10^6 cells/mL, no transfection and VLP production was observed (Figures 1A and 1B), although containing enough carbon source substrate. Both glucose and lactate concentrations were still approximately 2 g/L in the culture medium (Figure 1D). As a result, energy depletion was ruled out as a possible cause of the CDE. To further investigate the potential source of the problem, cells originally at 8 and 12 $\times$ 10^6 cells/mL were transfected after a complete MR step with fresh culture medium, removing any possible interference or metabolic by-products from the extracellular medium. This resulted in a significant increase in transfection efficiencies, although remaining significantly below the values observed when transfecting at 2 $\times$ 10^6 cells/mL (Figures 1E and 1F). When diluting the cultures at 8 $\times$ 10^6 and 12 $\times$ 10^6 cells/mL with fresh medium down to 2 $\times$ 10^6 cells/mL prior to transfection, transfection efficiencies significantly increased. This suggested that the fact of diluting the cells was also influencing the transfection efficiency, not only the removal of by-products and nutrient supplementation provided by the fresh MR. VLP cell-specific productivity was also different with and without dilution. Diluting from 12$\times$ 10^6 to 2 $\times$ 10^6 cells/mL still did not produce any VLP, suggesting that changes in cell physiology at HCD were playing a role in the CDE, regardless of the nutrient renewal and removal of extracellular inhibitors. Diluting from 8 $\times$ 10^6 to 2 $\times$ 10^6 cells/mL produced similar results, exhibiting a clear reduction in specific productivity compared with the 2 $\times$ 10^6 cells/mL control (Figure 1F). Transfections were also carried out concentrating cells originally at 2 $\times$ 10^6 up to 8 $\times$ 10^6 and 12 $\times$ 10^6 cells/mL. When concentrating from 2 $\times$ 10^6 to 8 $\times$ 10^6 cells/mL, the same transfection efficiency values than transfecting at 8 $\times$ 10^6 cells/mL after a fresh MR were obtained

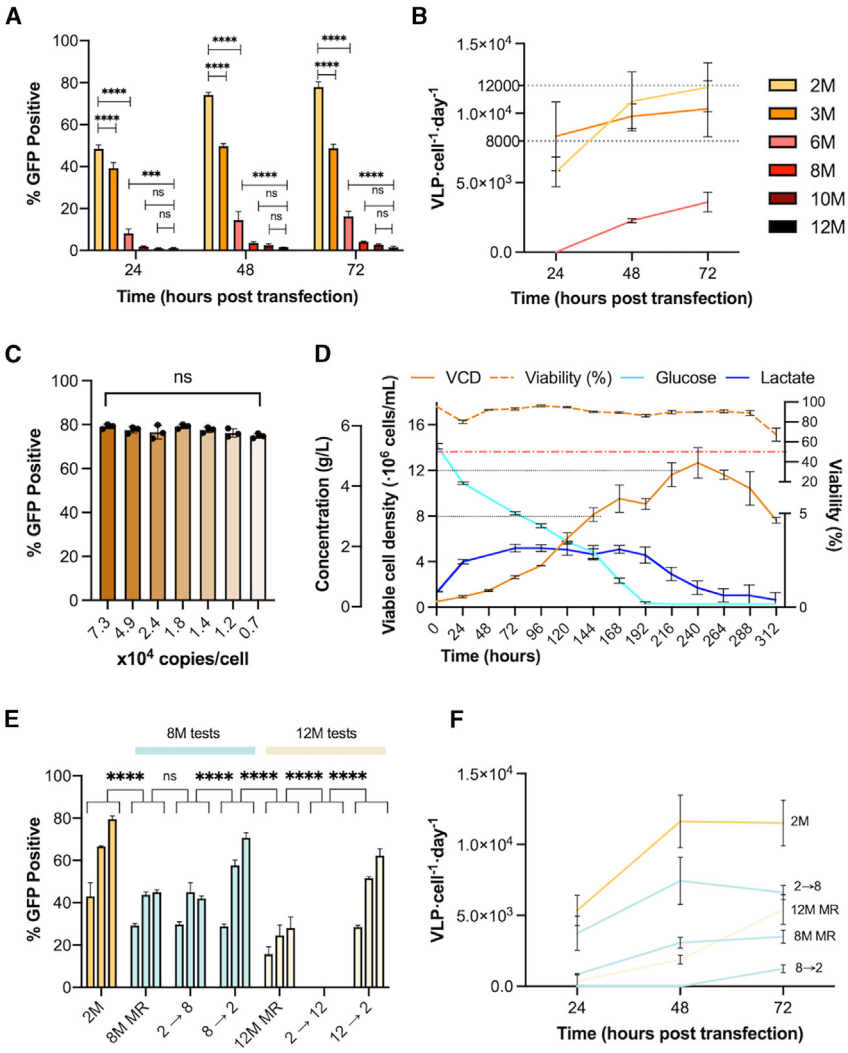

Figure 1. Characterization of the CDE

(A) Transfection efficiency measured in percentage of GFP-positive cells at different cell densities with no MR. (B) VLP cell-specific productivities at different cell densities. "M" represents million cells/mL. Values for the 8M, 10M, and 12M groups are 0 for all time points in this plot. (C) Transfection efficiency measured in percentage of GFP-positive cells. Transfections carried out at 2 × 10^6 cells/mL with decreasing copies of pGag::eGFP plasmid. pGag::eGFP copies were adjusted and stuffer mock plasmid DNA was used to reach a total of 1 μg/mL of total DNA for all conditions. (D) Growth curve of HEK293 cultured in HyCell TransFx-H culture medium. Red dotted line represents 50% of viability. Black dotted line represent 8 × 10^6 and 12 × 10^6 cells/mL (8M and 12M) points. Viable cell density is plotted in solid orange on the primary left y axis. Glucose and lactate concentrations are plotted in light and dark blue, respectively, on the secondary y axis. Cell viability is plotted in dotted orange on the right y axis. (E) Transfection efficiency tested at 8 and 12 × 10^6 cells/mL carrying out a complete MR with fresh medium, concentrating cells from 2 × 10^6 to 8 × 10^6 and 12 × 10^6 cells/mL, respectively (2→8 and 2→12), and diluting cells from 8 × 10^6 and 12 × 10^6 to 2 × 10^6 cells/mL (8→2 and 12→2) prior to transfection. The three bars represent 24, 48, and 72 hpt. (F) VLP cell-specific productivities measured in the different conditions tested in (E). Error bars represent standard deviation from biological triplicates. Significance was calculated using one-way ANOVA and Tukey's test. * p value < 0.05; *** p value < 0.001; **** p value < 0.0001.

(Figure 1E). Interestingly, when concentrating from 2 × 10^6 to 12 × 10^6 cells/mL, no transfection was achieved (Figure 1E). With renewed fresh medium in all cases, micronutrient depletion was discarded as a possible source of the problem. Cell-specific productivity was observed to decrease at HCD, even when concentrating metabolically active cells at 2 × 10^6 cells/mL with available fresh culture medium (Figure 1F). These results confirmed the existence of a two-factor contribution toward the CDE, establishing the framework for all further experiments. The two observed components of the CDE were individually studied: the inhibitory effect of the extracellular medium and the physiological state of the cell culture at HCD. This includes signaling molecules that could trigger a physiological change when cells reach HCD by natural growth or concentration.

Cells increase EV production upon fresh MR

To investigate the contribution of the extracellular medium to the CDE, transfections were carried out at 2 × 10^6 cells/mL, replacing the medium at the moment of transfection with different percentages of exhausted medium recovered from a 12 × 10^6 cells/mL culture (Figure 2A). As the percentage of exhausted medium increased, transfection efficiency at 2 × 10^6 cells/mL drastically decreased. It dropped from 80% down to 5%–7% when using more than 50% of conditioned medium from a 12 × 10^6 cells/mL culture. Notably, when more than 50% of conditioned medium was replaced, VLP production was completely inhibited. Interestingly, completely replacing the conditioned medium of 2 × 10^6 cells/mL with that of 12 × 10^6 cells/mL, resulted in a 2-fold increase in EV production at 72 h post transfection (hpt) (Figure 2B).

To study the effect of conditioned MR on EV production in a non-transfected culture, MR experiments were performed using different percentages of exhausted medium at 2 × 10^6 cells/mL, and total particle concentration in the extracellular medium was measured by NTA at 12 and 24 h post MR. It was observed that cells actively contribute to an increase in EV concentration in the extracellular medium upon fresh MR. EV volumetric productivity, calculated using total particles NTA measurements, showed that with higher percentages of fresh MR, EV productivity increased more rapidly from 12 to 24 h post MR. Using lower percentages of spent medium, 0%, 25%, and 50%,

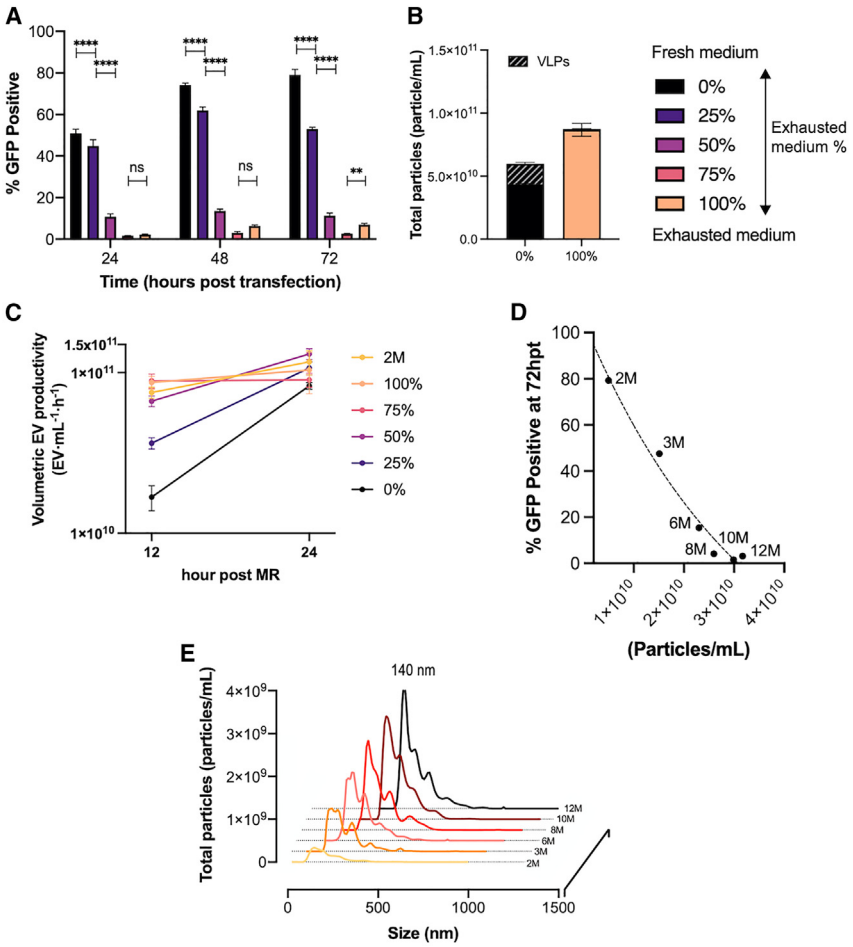

Figure 2. Study of EV production upon exhausted MR

(A) Transfection efficiency after MR with an increasing percentage of exhausted medium. The 0% condition represents an MR with fresh medium. (B) Concentration of total particles produced at 72 hpt when transfection was carried out after an MR step of 0% and 100% exhausted medium. When transfecting upon 0% MR, VLPs and EVs are coproduced. VLPs (hatched gray) represent ~27% of all particles produced. When transfecting upon 100% MR, no VLPs are produced and only EVs are measured. (C) EV volumetric productivity upon MR of different percentages of exhausted medium. Total particle concentration measured by NTA at 12- and 24-h port MR with increasing percentage of exhausted medium was used to calculate EV volumetric productivity (EV mL^{-1} h^{-1}). The control condition at 2×10^6 cells/mL was carried out without an MR. (D) Transfection efficiency measured by percentage of GFP-positive cells as the total particle concentration in the extracellular medium at the time of transfection and the cell density increased. (E) Characterization of EVs using nanoparticle tracking analysis (NTA) of produced EVs at different cell densities. Error bars represent standard deviation from biological triplicates. Significance was calculated using one-way ANOVA and Tukey's test. ** p value < 0.01; **** p value < 0.0001.

the achieved EV productivity increased more rapidly from 12 to 24 h post MR compared with 75%, 100%, and the 2×10^6 cells/mL control. EV volumetric productivity increased with higher fresh MR ratios. For higher percentage of exhausted MR, EV productivity remained constant or slightly increased from 12 to 24 h post MR (Figure 2C). Regardless of the MR performed, all cultures tended to reach similar particle concentration at 24 h post MR, suggesting that after an MR that removes all EVs from the extracellular medium, cells adjust their EV production and regulate the extracellular concentration required for cell-to-cell communication. All conditions reached a productivity of 1×10^{11} EV mL^{-1} h^{-1} at 24 h post MR (Figure 2C). Consistently, extracellular particle concentration at the time of transfection increased with cell density (Figures 2D and 2E). EV concentration was higher than 2×10^{10} particle/mL from 6×10^6 cells/mL onward and correlated with the previously observed decreased in transfection efficiency (Figure 1A).

Presence of EVs induced breakdown of DNA:PEI polyplexes

The interaction of EVs and DNA:PEI polyplexes was studied following two different approaches. First, DNA and PEI were added to conditioned medium coming from 12×10^6 cells/mL culture at different percentages to study the role and interaction of EVs in the process of complexation (Figure 3A). Second, DNA:PEI polyplexes were formed in fresh medium avoiding EV interaction and were then exposed to different percentages of exhausted medium (Figure 3B). After incubation, polyplexes were observed using cryogenic transmission electron microscopy (cryo-TEM) and used for transfection at 2×10^6 cells/mL. Both approaches led to polyplex break down and disruption (Figures 3C and S1C–S1F). The presence of EVs in the extracellular medium during and after complexation led to the reduction in size and electrodensity of the DNA:PEI polyplexes, while EV-polyplex aggregates appeared in both cases. There was no significant difference in polyplex size reduction depending on the treatment. Only the size of EV-polyplex aggregates was significantly different between treatments when using 50%, 75%, and 100% spent medium. In these cases, aggregates appearing when polyplexes were formed in spent medium were significantly larger than the ones appearing when exposing already formed polyplexes to the same spent medium. This might be due to the fact that PEI could have more available charges to interact both with DNA and EVs while forming the polyplexes than when the polyplexes are already formed. Fewer available charges could lead to smaller aggregates. However, both approaches led to dysfunctional polyplexes, obtaining the same results in transfection efficiency when they were used (Figures 3C, S1C, and S1D). The size of these macro-aggregates increased with higher percentages of exhausted medium. In turn, the size of DNA:PEI polyplexes was observed to decrease with exposure to increasing percentages of exhausted medium. When these

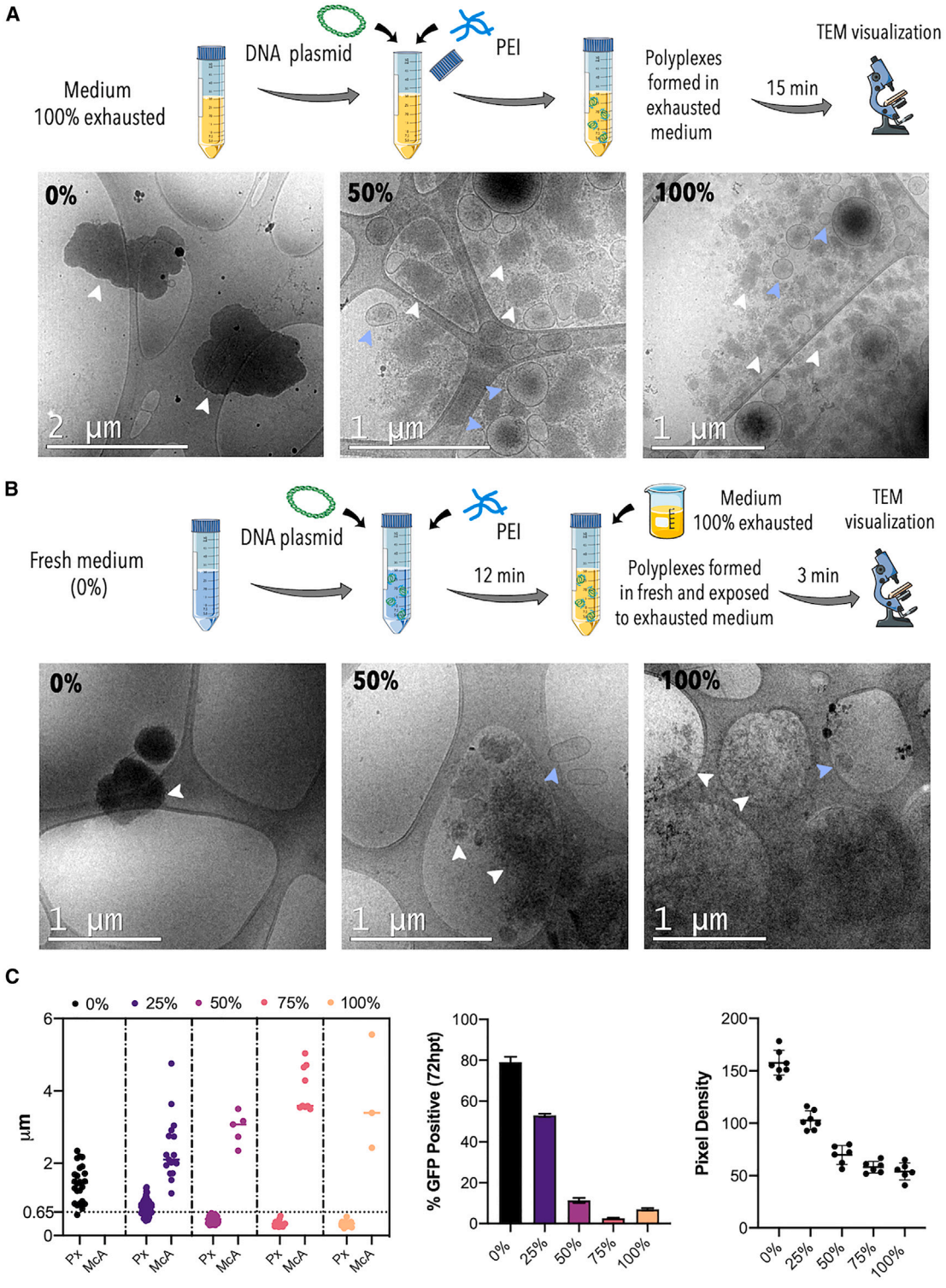

(legend on next page)

polyplexes were used for transfection, it led to a drastic reduction in transfection efficiency when polyplexes were smaller than 0.65 μm in diameter (Figure 3C). These results were corroborated by dynamic light scattering (DLS) analysis, where the appearance of a subpopulation of several microns was detected at increasing percentages of exhausted medium (Figures S1K and S1L). The macroaggregates that led to polyplex disruption were mostly formed by the interaction of the polyplexes with EVs present in the spent medium to which they were exposed (Figures 3A and 3B). This suggested that the polyplex breakdown and decrease in size observed in the samples that led to a reduction in transfection efficiency were caused by EV interaction.

Removing EVs from conditioned medium of HCD cultures restored transfection efficiency

To investigate the inhibitory role of EVs on transfection efficiency, EVs were completely removed from the conditioned medium of a 12×10^6 cells/mL culture, which was then used for transfection. To identify the specific EV population responsible for the inhibitory effect, different EV fractions were isolated and characterized. Sequential centrifugation steps based on the fractionation protocol described by Hiraga et al.,[41] along with a final anionic exchange (AEX) chromatography step, were employed to obtain four different EV fractions. These fractions included EVs pelleted at 10,000 × *g*, at 17,000 × *g*, and at 160,000 × *g*, as well as those retained in the AEX chromatography column (Figures 4A and 4B). The final AEX step was included to remove the remaining small EVs after the centrifugation steps. Transfections were conducted at 2×10^6 cells/mL following a complete MR step using each of the isolated EV fractions, resuspended in fresh medium at an equal final particle concentration. When studying the effect on transfection of each of the purified EV fractions, particle concentration was normalized prior to MR to the EV concentration found in the extracellular medium of a culture at 12×10^6 cells/mL, around 3×10^{10} particle/mL. The presence of EVs coming from the 10,000 × *g* and 17,000 × *g* fractions resulted in a 50% reduction in transfection efficiency. EVs from the 160,000 × *g* fraction caused an 88% reduction, while EVs coming from the chromatography column retentate completely inhibited transfection (Figure 4C). Notably, when cells at 2×10^6 cells/mL were transfected with the purified EV-depleted medium obtained from the fractionation process, transfection efficiency was fully restored (Figure 4C). This reversal of the previously observed transfection inhibition in conditioned medium from a 12×10^6 cells/mL culture (Figure 2A) was achieved despite the absence of glucose in the EV-depleted medium. According to the minimal information for studies of EVs 2018 (MISEV2018) guidelines,[42] a complete depletion of EVs is impossible, and only partial separation can be achieved. In this case, the obtained EV-depleted medium still contained 8×10^7 particles/mL, representing a 99.8% depletion of EVs and a reduction in all studied EV protein markers (Figures 4B, S2A, and S5). Remarkably, VLP production at 2×10^6 cells/mL improved by 60% (Figure S2C) and extracellular fluorescence increased by approximately 20% when conditioned medium was replaced with EV-depleted medium (Figure 4D), thereby enhancing VLP budding (Figure S2F). Importantly, the quality of the produced VLPs was maintained, as demonstrated by the consistent fluorescent particle size distribution profile (Figures S2D–S2G). EV-depleted medium did not induce higher Gag monomer rate production at 2×10^6 cell/mL, demonstrating that transfection could sustain VLP production solely through the presence of residual lactate (Figure 4A). Interestingly, when polyplexes were formed in EV-depleted medium and subsequently exposed to EVs, little to no effect was observed, as if this medium buffered the macroaggregation capacity of EVs (Figures S1C–S1F). In addition, when cell cultures at 12×10^6 cells/mL were transfected using EV-depleted medium, similar transfection efficiencies were obtained as with fresh MR (Figure 4E). It should be noted that the transfection efficiency did not reach the standard value observed at 2×10^6 cells/mL cultures, as the inhibitory element of the extracellular medium is only one component of the CDE, and the physiological component remained unmodulated in this case.

Proteomic identification of the most inhibitory fraction revealed five major protein clusters

The inhibitory EV fraction obtained from the chromatography column retentate transfection was characterized by LC-MS/MS proteomic analysis identifying a total of 1,181 proteins, of which 387 were identified with more than 1 peptide (Table S1). The functional enrichment analysis of these proteins revealed five major protein clusters: cell adhesion, extracellular matrix, anti-apoptotic, protein folding, and mRNA splicing (Figure S3). The most significantly enriched biological process was cell adhesion ($p = 3.3 \times 10^{-10}$), including proteins such as nidogen-2, tenascin, and cadherin-2, among others. The presence of matrix-degrading enzymes such as ADAM metallopeptidases 9 and 22 was also notable. The enriched biological process of extracellular matrix organization ($p = 4.1 \times 10^{-4}$) contained proteoglycans such as perlecan or distroglycan. Many other accessory matrix proteins such as fibulin, fibrillin, and collagen were also associated with cell adhesion gene ontology (GO) term. Also, anti-apoptotic GO term was enriched ($p = 1.4 \times 10^{-3}$) sharing many proteins with cell adhesion GO term. Cell adhesion and matrix metabolization signaling molecules are related to cell growth and migration. Protein folding enzymes such as cochaperones, heat shock proteins, and disulfide isomerases were also highly abundant in the eluted sample

Figure 3. Study of the interaction between DNA:PEI polyplexes and EVs in the exhausted medium

White arrows point to DNA:PEI polyplexes. Blue arrows point to EVs.

(A) Preparation of polyplexes directly in exhausted culture medium. Complexation medium for polyplex formation varied from 100% exhausted medium, 75%, 50%, 25%, and 0%. The control condition of complete fresh medium is noted as 0%. (B) Preparation of polyplexes in fresh medium (0%) followed by addition of exhausted medium once DNA and PEI are complexed. (C) Characterization of the DNA/PEI polyplexes (Px) and macroaggregates (McA) comprising EVs. Size of both Px and McA formed using the strategy from (A) in all different ratios of fresh/exhausted media (left). Transfection efficiency using these polyplexes (center). Polyplex electrodensity (right). For a total of 55 TEM micrographs. Error bars represent standard deviation from biological triplicates.

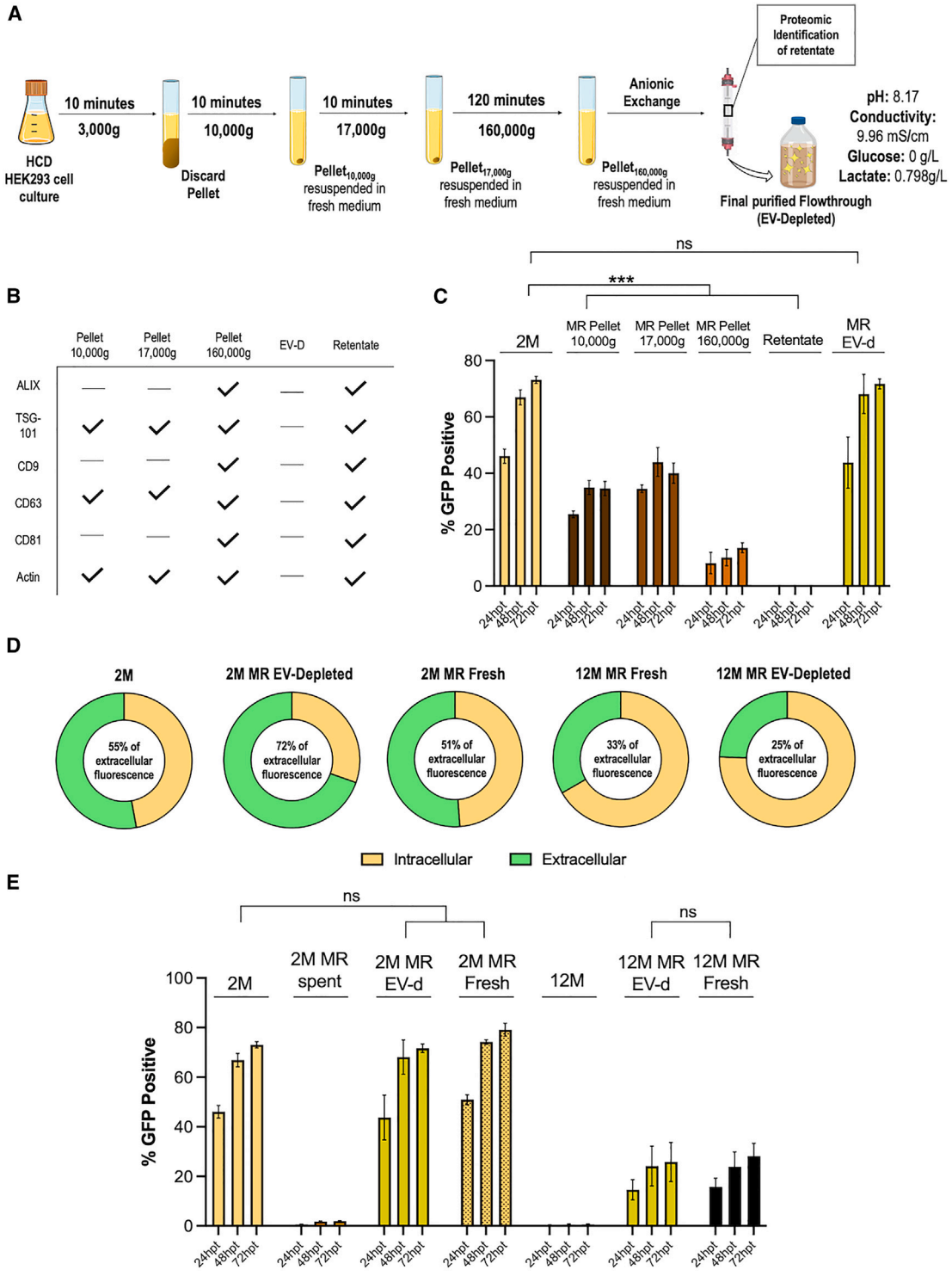

Figure 4. Effect of the EV-depleted medium

(A) Fractionation of exhausted medium coming from 12 × 10^6 cells/mL by sequential centrifugation and anionic exchange chromatography. (B) Table of EV markers contained in each pellet fraction. (C) Transfection efficiency achieved using the different fraction samples. (D) Ratio of extracellular to intracellular fluorescence in the different studied conditions. (E) Transfection efficiency in the different studied conditions. All experiments were performed using biological triplicates. LCD, low cell density; HCD, high cell density; MR, media replacement; EV, extracellular vesicle; M, million cells/mL. Error bars represent standard deviation from biological triplicates. Significance was calculated using one-way ANOVA and Tukey's test. *** p value < 0.001.

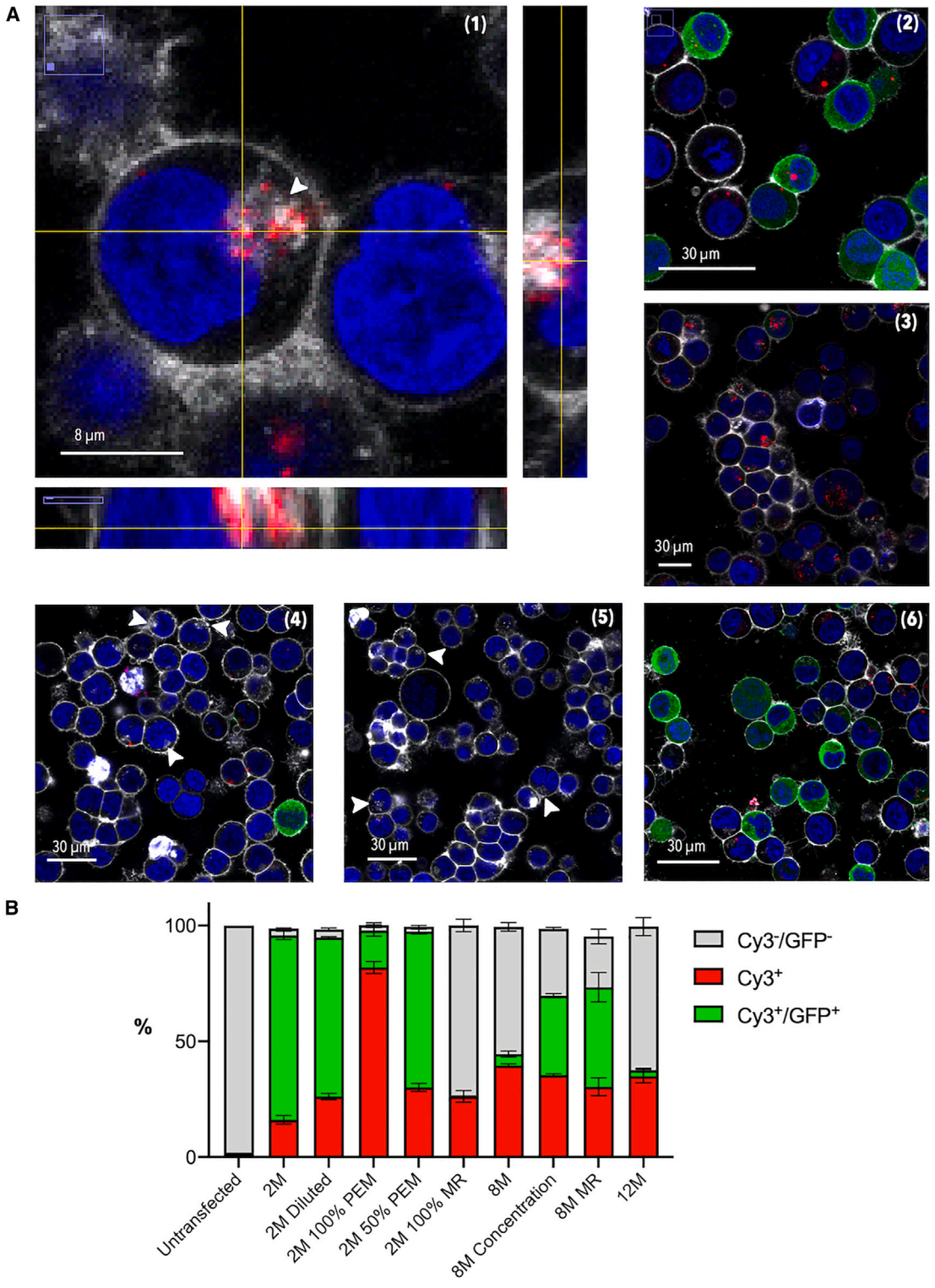

Figure 5. DNA:PEI polyplex intracellular trafficking in HEK293 cells

Blue, Hoechst, staining nuclei; red, Cy3-labeled pGag::eGFP plasmid DNA forming polyplexes (Px); white: CellMask, staining the cell membrane; green, eGFP coming from Gag::eGFP monomers in VLP-producing conditions. (A) Confocal microscopy images taken at 24 hpt. (1) Transfection at 2 × 10^6 cells/mL with Px were formed in 100% of

(legend continued on next page)

($p = 2.7 \times 10^{-8}$), acting as homeostasis regulators, avoiding accumulation of misfolded proteins and contributing to the anti-apoptotic signaling. The presence of proteins annotated with mRNA splicing GO term ($p = 3.2 \times 10^{-5}$) suggested that retained EVs contribute to RNA process modulation as part of the cell-to-cell communication functions. These results indicated that EVs act both as a physical barrier and as an inductor of physiological changes through protein interaction to converge in what is reported as the CDE, in accordance to previously reported works. Hence, complete EV depletion was able to restore transfection (Figure 4).

Polyplexes are sequestered in intracellular vesicles at HCD preventing transfection

To study the component of the CDE related to the physiological state of cell cultures at HCD, 8 and 12×10^6 cells/mL cultures were visualized using confocal microscopy upon transfection using DNA labeled with Cy3. All confocal experiments utilized CellMask for visualizing the plasma membrane (white in the confocal images), Cy3 for labeling the transfected DNA (red in the confocal images), Hoechst staining nuclei (blue in the confocal images), and green fluorescence from GFP in the Gag::eGFP monomers. At HCD, intracellular membranous structures were observed to colocalize with DNA:PEI polyplexes as shown in Figures 5A and S4. Interestingly, these macroaggregates of polyplexes and membranous structures appeared in cultures at 2×10^6 cells/mL when the conditioned medium was replaced with exhausted medium coming from 12×10^6 cells/mL cultures and when the polyplexes were formed in exhausted medium (Figure 5A). These intracellular structures sequestered the polyplexes, preventing them from entering the nucleus and thereby preventing transfection. Similarly, these membranous macroaggregates also were observed in the pericellular space (Figures 5A and S4), resembling the macroaggregates observed in cryo-TEM when exposing DNA:PEI polyplexes to EVs (Figure 3). These results suggest that EVs were sequestering and blocking DNA:PEI polyplexes in the extracellular medium, preventing them from reaching the cell. Moreover, the intracellular membranous structures observed at HCD captured polyplexes in the cytosol, contributing to the reduction in transfection efficiency. Interestingly, polyplexes formed in exhausted medium were taken up by cells in the same proportion as polyplexes formed in fresh medium. However, they remained unexpressed, captured in the intracellular membranous macroaggregates (Figures 5A and 5B). Furthermore, when performing an MR step with 100% exhausted medium prior to transfection, only approximately 25% of polyplexes were able to enter the cell, while remaining unexpressed (Figure 5B). A similar percentage of polyplexes entered the cell and remained unexpressed at 8 and 12×10^6 cells/mL. Interestingly, when replacing the conditioned medium with fresh medium, the total percentage of polyplexes increased to approximately 75% but still about 25% remained unexpressed, localized in intracellular membranous structures (Figures 5A and 5B). The additional 50% was due to the fresh MR step. This is consistent with the proposed two-step mechanism of polyplex sequestration by EVs, at the extracellular and intracellular medium. These results corroborated that the two components of the CDE could be modulated independently. Consequently, when concentrating from 2 to 8×10^6 cells/mL and transfecting prior to a fresh MR, the intracellular membranous structures still appeared (Figures 5A and 5B), emulating natural cell density growth and reducing transfection efficiency.

UDP-glucose ceramide glucosyltransferase overexpression affected intracellular vesicle formation, releasing polyplexes and improving transfection at HCD

UDP-glucose ceramide glucosyltransferase (UGCG) overexpression was selected based on previous reported studies[24,43] due to its effect on increasing transfection efficiency and affecting the formation of intracellular vesicles. Knocking out the *ugcg* gene has been reported to block infection of endosome-entering viruses, confining infective particles in intracellular structures.[44–46] Thus, we hypothesized that overexpressing this enzyme could reduce intracellular polyplex sequestration at HCD. To test if UGCG played a role in eliminating the intracellular bottleneck for transfection, UGCG was overexpressed by transient transfection at 2×10^6 cells/mL followed 4 h later by co-transfection of Gag::eGFP whose polyplexes were formed in exhausted medium to emulate HCD. Transfection efficiency significantly increased and the previously observed intracellular membranous structures were not detected (Figures 6A and 6B). Furthermore, cotransfecting both UGCG and Gag::eGFP after a fresh MR and forming the polyplexes in fresh medium, resulted in a further increase in transfection efficiency (Figure 6A). To finally test the ability of UGCG overexpression to improve transfection at HCD, 12×10^6 cells/mL cultures were co-transfected with both UGCG and Gag::eGFP after a fresh MR, obtaining a significant increase in transfection efficiency at 24, 48, and 72 hpt, reaching more than 40% and proving that the cellular component of the CDE could be addressed. Nonetheless, the standard transfection efficiency of 2×10^6 cells/mL could not be achieved due to the inherent limitations of the CDE at HCD, as UGCG overexpression was carried out using TGE itself. These results confirmed that UGCG overexpression affected intracellular vesicle formation, releasing polyplexes and improving transfection at HCD.

Modulation of UGCG expression and EV depletion improved cell-specific virus yield infection of AdV 5

UGCG overexpression and EV depletion were also tested for AdV 5 production via infection. UGCG was transiently overexpressed 4 h

exhausted medium. Analysis of orthogonal views to verify intracellular colocalization of Px (Cy3-labeled DNA) and endocytosed membranous structures, indicated by white arrows (membranes stained with CellMask). (2) Standard transfection at 2×10^6 cells/mL with Px formed in fresh medium. Gag::eGFP production can be observed. (3) Transfection at 2×10^6 cells/mL with Px formed in 100% of exhausted medium. (4) Transfection at 8×10^6 cells/mL with Px formed in fresh medium. (5) Transfection at 2×10^6 cells/mL after a complete MR with exhausted medium and Px formed in fresh medium. (6) Transfection at 2×10^6 cells/mL after MR with EV-depleted medium and Px formed in fresh medium. (B) Quantification of the $Cy3^-/GFP^-$, $Cy3^+$, and $Cy3^+/GFP^+$ populations by flow cytometry in the different studied conditions. Error bars represent standard deviation from biological triplicates. PEI, polyethylenimine; hpt, hours post transfection; PEM, polyplexes formed in exhausted medium; M, million cells/mL.

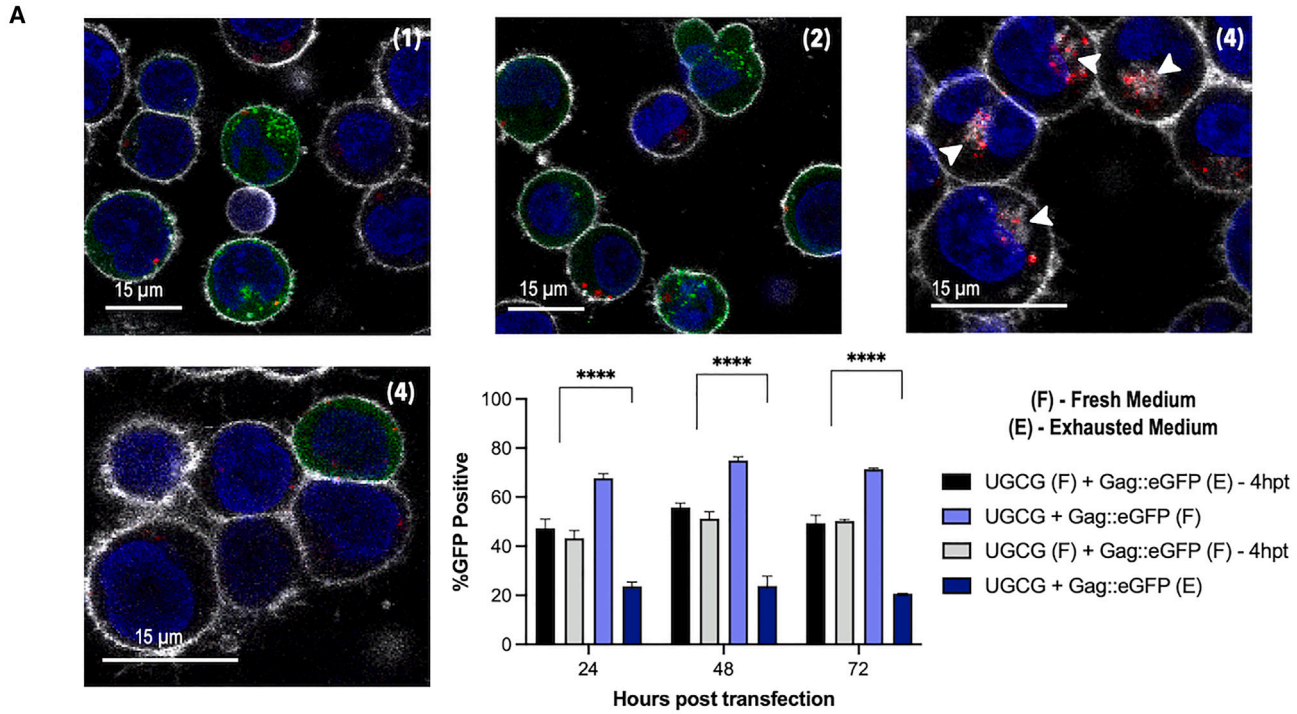

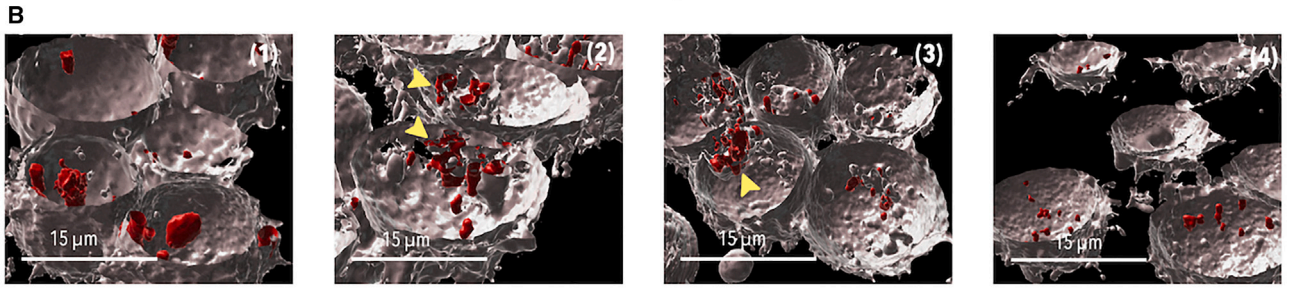

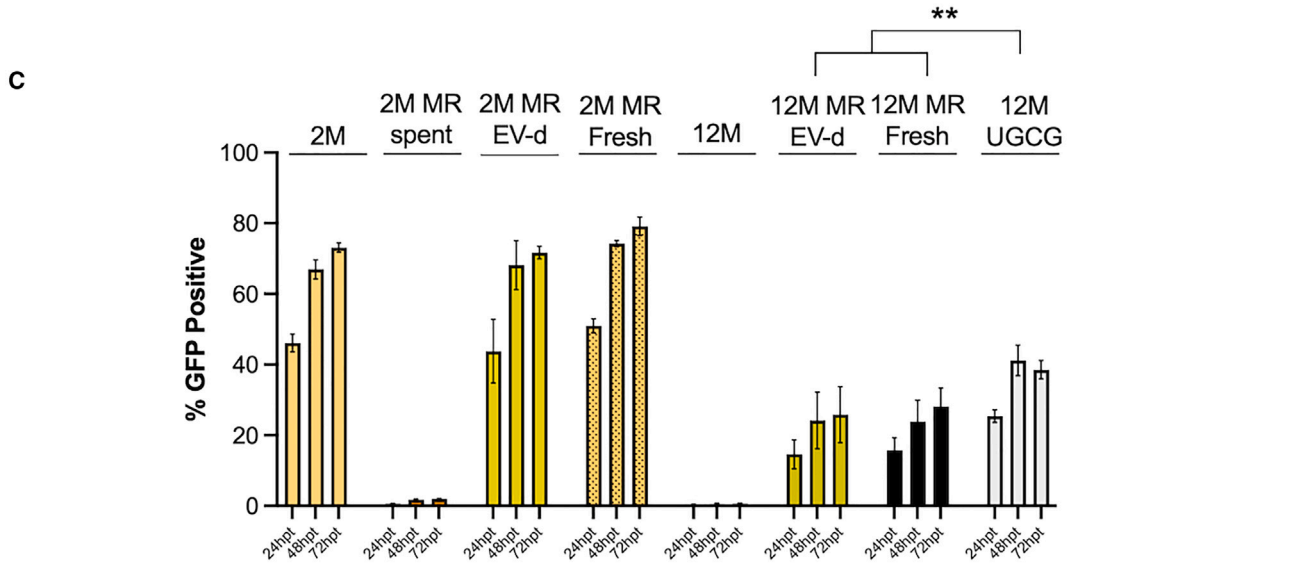

(legend on next page)

prior to infection and the corresponding MRs were performed immediately before infection. All tested conditions are presented in Figure 7. When infecting at 1 and 2 × 10^6 cells/mL, similar virus yields of approximately 25,000 vector genomes (vg)/cell were obtained. Consistent with the CDE, virus yield decreased to around 100 vg/cell when infecting at 12 × 10^6 cells/mL. Unfortunately, incorporating a transfection step prior to infection significantly reduced virus yield regardless of the transfected plasmid, as shown using a mock plasmid (pMock). Transiently transfecting UGCG showed no significant difference in titers compared with pMock transfection at 2 × 10^6 cells/mL. However, at 12 × 10^6 cells/mL, UGCG overexpression significantly increased virus titers compared with infection after pMock transfection, from 2 to 150 vg/cell. This suggested that UGCG could also potentially alleviate the intracellular component of the CDE also in Adv 5 production via infection. Moreover, a complete fresh MR only improved titers when infecting at 2 × 10^6 cells/mL. Depleting EVs from exhausted conditioned medium significantly reduced virus yield at 2 × 10^6 cells/mL, representing a notable change compared with the results observed in transfection experiments. However, at 12 × 10^6 cells/mL, EV depletion had no effect on virus titer.

DISCUSSION

Exhausted medium fractionation leads to different degrees of inhibition depending on EV population

Cell culture media have been shown to greatly influence the charge of DNA:PEI polyplexes and thereby alter their stability in the extracellular medium.[47] Polyplex populations of micrometric dimensions promote proper cellular uptake, resulting in higher transfection rates.[48] In this work, we observed a clear polyplex disruption in conditioned medium due to their interaction with EVs associated to cell growth. As shown, EVs induce extensive aggregation of polyplexes, compromising transfection. However, molecular EV-polyplex interactions driving this phenomenon need to be investigated to further understand their physicochemical nature.

The term EV comprises a wide range of heterogeneous vesicle populations formed by microvesicles, exosomes, oncosomes, apoptotic bodies, mitovesicles, and others.[27,38] They can be classified upon their biogenesis pathway, size, cargo, and biochemical characteristics.[49] However, the boundaries between the different types of EVs are not well defined and, according to MISEV2018 guidelines, thorough characterization is required to accurately identify the specific type of EV.[42] For this work, the specific type of EV in each of the different fraction was not characterized, as it goes beyond the scope of this investigation. For this purpose, EV subpopulations were only separated regarding the sedimentation speed and the protein markers of each of the fractionation steps. All studied EV fractions had similar size distribution profiles, with diameters ranging from 150 to 350 nm (Figure S2). Five of the most common protein markers used for EV characterization were used for all fractions: TSG-101, ALIX, CD9, CD63, and CD81. Notably, all markers only appeared in the 160,000 × *g* fraction and the retentate, which led to the highest reduction in transfection efficiency. These markers are related to small EVs, typically derived from endosomal biogenesis.[38] Transfection efficiency is substantially or completely reduced when using both the 160,000 × *g* and the retentate fraction for transfection, suggesting that the inhibitory elements have an endosomal origin and might be secreted in the form of exosomes or small EVs. Furthermore, elements that reduce the density of the vesicles, such as protein glycosylation, might be purified in this EV fraction and also contribute to the CDE. In addition, many of the identified proteins present in the retentate fraction, such as heat shock and RNA-binding families are reported to be found in exosomes.[50,51] Nonetheless, microvesicles and exosomes share common characteristics, but lack distinct defining features.[52] Further investigation and characterization of the different EV populations will be required to define whether exsosomes are responsible for the CDE.

Interestingly, reported works on HCD infection of AGE1.CR cells to produce influenza virus in perfusion showed that removing small EVs retained in the bioreactor alleviated the CDE, improving specific virus yield. Increasing the pore size of the hollow fiber module from 0.2 to 0.5 μm in the cell retention device for infection at a cell density of 25 × 10^6 cells/mL increased specific virus yield. The specific virus yield rose from 518 to 1,708 virions/cell.[18]

However, when depleting the extracellular medium of both large and small EVs, there was a significant decrease in Adv5 yield (Figure 7), suggesting that different EVs have a different role in the process of infection. The difference regarding how EVs influence both transfection and infection processes remains uncharacterized.

VLP budding is enhanced upon MR with EV-depleted medium despite absence of macronutrients

Replacing the conditioned medium with EV-depleted medium at 2 × 10^6 cells/mL before transfection resulted in 60% increase in

Figure 6. Effect of UGCG in transfection

Blue, Hoechst, staining nuclei; red, Cy3-labeled pGag::eGFP plasmid DNA forming polyplexes (Px); white, CellMask, staining the cell membrane; green, eGFP coming from Gag::eGFP monomers in VLP-producing conditions. Intracellular membranous structures are indicated by white arrows. (A) Confocal microscopy images of transfections performed after a fresh MR step at 2 × 106 cells/mL. (1) Transfection of UGCG with Px formed in fresh medium followed by transfection with Gag::eGFP at 4 hpt with Px formed in exhausted medium. (2) Co-transfection of UGCG and Gag::eGFP with Px formed in fresh medium. (3) Co-transfection of UGCG and Gag:eGFP with Px formed in exhausted medium. (4) Co-transfection of UGCG and Gag::eGFP with Px formed in fresh medium at 8 × 10^6 cells/mL. Graph: transfection efficiency of cotransfections with UGCG and Gag::eGFP with Px formed either in fresh or exhausted medium. (B) 3D deconvolution of confocal microscopy images with IMARIS of (1) standard transfection, (2) Gag::eGFP with Px formed in exhausted medium, (3) UGCG + Gag::eGFP with Px formed in exhausted medium, and (4) UGCG + Gag::eGFP with Px formed in fresh medium. Intracellular membranous structures are indicated by yellow arrows. (C) Transfection efficiency of all studied conditions, including at 12 × 10^6 cells/mL with EV-depleted medium and UGCG cotransfection. Error bars represent standard deviation from biological triplicates. Significance was calculated using one-way ANOVA and Tukey's test. ** p value < 0.01; **** p value < 0.0001. UGCG, ceramide glucosyltransferase; CDE, cell density effect; MR, medium replacement; M, million cells; Px, polyplexes.

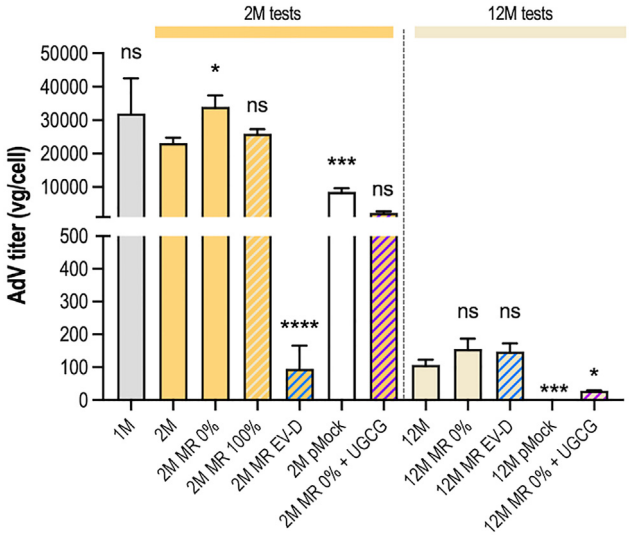

Figure 7. Adenovirus titer (vg/cell) in HEK293 after infection of AdV 5 under the different studied conditions

MR with complete fresh medium is notated as 0%. MR with complete exhausted medium is notated as 100%. Significance is calculated compared with 2M and 12M control conditions, respectively, in each group when no transfection is involved and for the pMock condition. Significance is calculated comparing to 2M-pMock and 12M-pMock when UGCG transfection is carried out in each condition, respectively. Error bars represent standard deviation from biological triplicates. Significance was calculated using one-way ANOVA and Tukey's test. * p value < 0.05; *** p value < 0.001; **** p value < 0.0001. MR, medium replacement; M, million cells/mL; EV-D, extracellular vesicle depleted.

VLP titers and 20% improvement in VLP budding efficiency (Figure 4). This effect could be attributed to the observed increased in volumetric productivity of EVs with fresh MR (Figure 2). All vesicles being depleted, the cellular shift toward EV production is most probably also stimulating the pathways for VLP production. Both VLPs and EVs utilize the endosomal sorting complexes required for transport complex and its accessory proteins as one of the primary secretion pathways.[53,54] Moreover, transfection itself has been reported to increase the biogenesis of small EVs, upregulating different proteins belonging to the endosomal pathway.[25] This might explain the increase in VLP titers observed when transfecting after EV-depleted MR. This suggests that implementing the strategy of increasing MR or perfusion rates in bioprocess development could effectively increase viral particles titers by depleting the extracellular medium of coproduced EVs. Interestingly, under these circumstances of depleting conditioned medium at 2×10^6 cells/mL of glucose, VLP production was still sustained during the phase of lactate co-metabolization. To the best of our knowledge, this is the first report of sustained transfection-based VLP production under carbon-limiting conditions. However, under these carbon-limiting conditions, VLP production and budding are inhibited at 12×10^6 cells/mL.

Interestingly, previous studies investigating molecular changes at increasing cell densities[24,55] observed a reduced retrograde transport at HCD. These alterations were observed in membrane-derived lipids such as diacylglycerols, phosphatidic acids, and cholesterol esters, and intracellular lipids such as lysophosphatidylethanolamines, as well as an overall downregulation of lipid biosynthesis.[51,56] Multi-omics studies upon MR with EV-depleted medium should be performed to analyze the main molecular changes related to increased intracellular budding.

Cell-to-cell communication mediated by EVs contributes to the CDE

Extracellular vesicles transport molecules of biological relevance (e.g., miRNAs, mRNAs, proteins, and DNA) as a means of cell-to-cell communication with the recipient cell.[57] Despite the discrepancies surrounding their biogenesis, loading pathways, and functions, EVs are a subject of increasing interest in the biomedicine field.[58] They are tightly connected to the extracellular matrix as the glycocalyx, which is highly enriched in glycoproteins and proteoglycans, and anchors EVs through tetherin-based interactions.[59] EVs contain metallopeptidase, oxidase, and glutaminase receptors that can interact with their surroundings and release their content, modifying nearby microenvironments.[58] Interestingly, when EVs are intentionally added to cell cultures by either performing an MR with exhausted medium or by co-addition with DNA:PEI polyplexes, culture morphology is altered. Here, cells aggregate and remain clustered similar to a tumorigenic environment.[60] These observations are aligned with reported cancer studies in which EV-induced production of extracellular matrix is critical for tumor formation and migration.[61–63] Consistently, the AEX retentate fraction was highly enriched in matrix proteins, peptidases, isomerases, and oxidases that could induce alterations in the extracellular matrix and disrupt polyplex internalization. Glyceraldehyde-3-phosphate dehydrogenase (GAPDH) has recently been identified as a master regulator of intracellular and extracellular EV clustering through its interaction with phosphatidylserine binding motifs.[64] Here, GAPDH has also been identified in the AEX retentate fraction. At increasing cell densities, EV signaling might be triggering aggregation to fit more new cells in the same volume. This hypothesis would explain the ability of the exhausted medium to mimic HCD cultivations and how EV depletion can restore morphology at low cell density.

Future potential applicability for manufacturing of TGE-based biopharmaceuticals

In addition, UGCG has been shown to alleviate intracellular EV clustering and enhance transfection. However, this effect was tested through TGE overexpression. Therefore, UGCG expression itself was intrinsically affected by the CDE. A 15% improvement in transfection efficiency was achieved considering that UGCG expression was itself limited. This is the main reason why we could not fully assess the potential of UGCG in alleviating the intracellular component of the CDE. To conduct a comprehensive evaluation, overexpression should be achieved without TGE. Establishing a stable cell line constitutively expressing UGCG would allow us to test its full effect on improving transient transfection at HCD. We expect that a cell platform with this characteristic, not presenting the intracellular component of the CDE, could present an improvement in transient

transfection higher than the obtained 15%. This platform could be used for transfection at HCD in large-scale manufacturing of TGE-based biologics. Nonetheless, UGCG is the precursor enzyme in the glycosphingolipid synthetic pathway, catalyzing the first step of glucosylceramide-based glycosphingolipids.[44,56,65] Therefore, constitutively overexpressing it could alter membrane fluidity and hamper culture viability and growth. Consequently, tuning UGCG expression by an inducible system could be the best option to design such a platform. A better understanding of the role of UGCG in intracellular vesicle modulation would allow specific genetic engineering approaches without compromising viability of the cultures.

As for bioprocess engineering, several variations of the classic perfusion approach have emerged in the last years,[66] broadening the possibilities of setting in complex processes that were unfeasible a decade ago. Still, elimination of the CDE at large scale could pose an engineering challenge if EV depletion is to be achieved at bioreactor scale. However, there is a high potential in the combination of both technical approaches for the removal of EVs and genetic engineering approaches for the generation of a platform overexpressing UGCG. The resulting biomanufacturing process could improve production for all TGE-based biologics, such as VLPs, lentiviruses, rAAVs, AdVs, etc. The procedures described here could be applied to any viral vector production platform. In our case, VLP cell-specific productivity transfecting at 12×10^6 cells/mL increased from 0 to around 3,000 VLPs cell^{-1} day^{-1} when depleting the extracellular medium from EVs (Figure S2). Moreover, when overexpressing UGCG at 12×10^6 cells/mL, VLP cell-specific productivity reached around 5000 VLPs cell^{-1} day^{-1}. Despite the effect of UGCG being only partial due to the CDE affecting its own overexpression as explained above, this increase already accounted for 42% of the desired cell-specific productivity observed at 2×10^6 cells/mL under standard transfection conditions.

This proved that modulating both the extracellular and intracellular components of the CDE improved transfection efficiency and cell-specific productivity at HCD by 45% and 42%, respectively. These promising results show room for improvement that could be certainly undertaken by further cell engineering strategies, as described already. The results obtained for HIV-1 Gag VLP production showed the potential applicability for similar viral vectors currently produced by transient transfection.

Interestingly, the results obtained when testing Adv5 infection showed that UGCG overexpression significantly improved viral titers at 12×10^6 cells/mL. However, the effect of transient transfection itself when testing UGCG hampered the infection process, reducing the potential of UGCG to alleviate the CDE. Regardless of the expressed gene, the transfection process causes an overall homeostasis disruption in the cell, altering up to 66 biological processes.[24] This general homeostasis disruption might hamper viral infection, thus reducing Adv viral titers if infection is carried out after transfection. To successfully test the effect of UGCG alleviating the CDE at HCD for production of Adv via infection, an inducible cell line will be required, skipping the transfection step for its overexpression. Therefore, further research on cell engineering is required and key to fully addressing the CDE in the different cell platforms at large scale.

Implications upon the novel findings of the molecular mechanisms in the CDE

In this work, the two components of the CDE have been independently identified and studied. The presence of EVs in the culture medium was proven to interfere with DNA:PEI polyplex uptake, causing their breakdown and macroaggregate formation together with EVs, thus reducing transfection efficiency. EV concentration in the culture medium increased at higher densities, emphasizing this effect. Importantly, not all EV populations were equally contributing to the CDE, showing distinct inhibition profiles. Depleting EVs from the extracellular medium restored transfection efficiency and enhanced VLP production by 60%. Moreover, the formation of intracellular membranous structures at HCD was observed to capture DNA:PEI polyplexes in the cytosol, preventing them from reaching the nucleus. These structures appeared at HCD and upon addition of EVs coming from an HCD conditioned medium. Finally, the overexpression of the enzyme UGCG reduced the intracellular membranous structures, releasing DNA:PEI polyplexes and improving transfection at HCD, partially overcoming the CDE. These modulations also improved cell-specific virus yield upon infection of AdV 5 at HCD, showing their potential to alleviate the CDE for different production systems. These results pave the way for future cell engineering strategies to test the full potential of UGCG overexpression at HCD. Moreover, identification of the main surface molecules that trigger the interaction between EVs and polyplexes could allow precise metabolic engineering strategies to further improve transfection, potentially overcoming the CDE at large scale and overall improving biomanufacturing.

MATERIALS AND METHODS

Cell line and culture conditions

The cell line used in this work is a serum-free suspension-adapted human embryonic kidney HEK293 (HEK293SF-3F6) cell line from the National Research Council of Canada (Montreal, Canada), kindly provided by Dr. Amine Kamen. Cells were routinely cultured in disposable polycarbonate 125 mL vented shake flasks (Corning, NY) and expanded when needed in 250 mL and 1 L vented shake flasks (Corning). Cells were kept in a Kuhner shaker LT-X (Kuhner, Birsfelden, Switzerland) at 37°C, 5% CO_2, and 85% RH at 130 rpm and passaged every 2–3 days at densities of $0.3–0.5 \times 10^6$ cells/mL with viabilities over 95% to ensure exponential phase maintenance. Culture medium was HyCell TransFx-H (GE Healthcare, Chicago, IL) supplemented with 4 mM GlutaMAX (Gibco, Thermo Fisher Scientific, San Jose, CA) and 0.1% Pluronic F-68 (Gibco). For low volume experiments, cells were cultured in low-attachment sterile 6-well plates (Thermo Fisher Scientific) with a final volume of 2 mL with the same culture conditions as described above.

Cell concentration and cell viability were determined using a NucleoCounter NC-3000 automatic (Chemometec, Allerod, Denmark) by properly following the manufacturer's instructions.

For the MR experiments, the appropriate cell culture volume was recovered by centrifugation at 300 × *g* for 5 min. Cell cultures were subjected to different rates of fresh and exhausted culture media that will be indicated in each experiment.

Transient transfection and protein expression

Standard transfections were performed at a cell density of 2×10^6 cells/mL using a final DNA concentration of 1 μg/mL with no MR, unless stated otherwise. The cationic transfection reagent used was PEIPro (PolyPlus, Illkirch-Graffenstaden, France). In brief, the corresponding amount of DNA was added in fresh culture medium (10% of the culture volume to be transfected) and vortexed for 10 s. Then, PEIPro was added in a ratio of 2:1 (PEI:DNA, w/w) and the mix was vortexed three times for 3 s followed by 15 min of incubation at room temperature (RT). Finally, the appropriate volume of transfection mixture was added to the cultures.

The plasmid used encoded the HIV-Gag polyprotein fused in frame to the eGFP under the same CMV enhancer and CMV promoter, henceforth noted as Gag::eGFP.

For the experiment involving stuffer DNA, the pGag::eGFP plasmid with a frameshift mutation preventing Gag::eGFP expression was used, noted as pMock. For variations to the standard transfection protocol, each change in the procedure is specified in the text.

For UGCG cotransfections, the same total DNA amount of 1 μg/mL was used, 50% of the plasmid coding for UGCG and 50% of the plasmid coding for Gag::eGFP.[43]

Flow cytometry

Sampling was performed at each specified time point and cells were fixed. In brief, samples were centrifuged for 5 min at 300 × *g*, and supernatants were discarded. The resulting pellets were fixed using formaldehyde 2% in PBS for 10 min at RT and then washed and resuspended with PBS for a final FACS analysis. BD FACS Canto Flow Cytometer (BD Biosciences, San Jose, CA) allowed the discrimination between GFP- and non-GFP-positive populations by light excitation at 488 nm. Results were then adjusted with FACS DIVA proprietary software. Experiments involving Cy3 fluorochrome were analyzed using a CytoFLEX LX (Beckman Coulter Life Sciences, Brea, CA) equipped with a laser at 649 nm, allowing the identification of Cy3-positive populations. Raw data were adjusted with proprietary CytExpert software (Beckman Coulter Life Sciences).

HIV-1 Gag VLP quantification: Fluorimetry

The concentration of HIV-1 Gag::eGFP VLPs was assessed by fluorimetry using an in-house-validated quantification assay.[67] Supernatants were recovered by centrifugation at 1,000 × *g* for 5 min. GFP intensity was measured employing a Cary Eclipse Fluorescence Spectrophotometer (Agilent Technologies). Relative fluorescence units (RFUs) resulted from the subtraction of non-transfected control samples to each transfected sample. These values were then converted to VLP concentration following the next equation:

$$\text{VLPs / mL} = (4.448 \times \text{RFU} - 63.3) \times 10^8 \quad \text{(Equation 1)}$$

HIV-1 Gag VLP and EV quantification: NTA

NTA was used to quantify both fluorescent and non-fluorescent diffracting particles. All measurements were carried out with a NanoSight LM 20 Device (NanoSight, Amesbury, UK) equipped with a blue laser (488 nm) to quantify Gag::eGFP VLPs and neutral density filter for total particle assessment by light scattering. Values were obtained as the mean of three independent measurements. Data were finally analyzed with NanoSight NTA 3.1 Software.

Sequential centrifugation: EV fractionation

Conditioned medium was fractionated with a four-step sequential centrifugation after 9 days of batch growth. In brief, cells were removed with a first centrifugation at 3,000 × *g* for 10 min. The recovered supernatant was centrifuged at 10,000 × *g* for 10 min. The subsequent recovered supernatant was centrifuged at 17,000 × *g* for 10 min. Finally, a volume of 25 mL of recovered clarified supernatant was ultracentrifuged at 160,000 × *g* for 2 h at 4°C using a 70Ti rotor in a Beckman Optima L100XP centrifuge (Brea). After ultracentrifugation, samples of each of the supernatants and pellets were recovered and stored at −80°C for future usage.

Anionic exchange chromatography: EV depletion

Supernatant coming from the last step of ultracentrifugation was purified with a prepacked 4.7 mL HiScreen Capto Q ImpRes column (Cytiva, GE Healthcare Live Sciences, Uppsala, Sweden) to capture EVs. Before loading, column was pre-equilibrated with 5 CV of 6% Buffer B (50 mM HEPES, 2 M NaCl [pH 7.2]) in Buffer A (50 mM HEPES [pH = 7.2]). Sample was directly injected into the column via the sample pump. After sample loading, the column was washed with 5 CV of 6% Buffer B. Elution was achieved by a salt step gradient consisting of 20 CV of 15%, 35%, 45%, and 65% Buffer B (300 mM NaCl, 700 mM NaCl, 900 mM NaCl, 1,300 mM NaCl). The column was regenerated with 5 CV of 100% Buffer B, and sanitization was performed with 2 CV of 1 M NaOH. Solutions were filtered using 0.22 μm filters. Chromatographic run was performed at 1.2 mL min^{-1} flow rate. Fractions of 1 mL were collected and pooled according to the chromatogram.

DNA labeling

Transfection DNA was labeled with Cy3 fluorochrome using a Label ITTracker Kit (Mirus Biotechnology, Madison, WI) according to the manufacturer's instructions. Protocol is succinctly described by Cervera et al.[68]

Confocal microscopy

Visualization of VLP-producing cells was performed using a FluoView FV 100 confocal microscope (Olympus, Tokyo, Japan). HEK293 cells were dyed with CellMask 10 mg/mL (Life Technologies, MA) and with Hoechst 10 mg/mL (Life Technologies, Carlsbad, CA). Excitation/emission parameters of each dye used for confocal

microscopy were 649 nm/666 nm for CellMask, 649 nm/670 nm for Cy3, 350 nm/461 nm for Hoechst, and 488 nm/510 nm for Gag::eGFP VLPs. In brief, 1 μL of each dye was mixed with 1 mL of cell culture followed by a 10 min incubation at RT protected from light. Samples were placed in glass-bottom dishes (MatTek, Gothenburg, Sweden) for visualization under the microscope. Images were treated with LAS AF software (Leica Microsystems, Wetzlar, Germany).

Cryo-TEM

Morphology and electron density of DNA:PEI polyplexes were studied in cryogenic conditions. After each specific treatment, the sample was immediately plunged into liquid ethane to instantly freeze it at −180°C. Approximately 2 μL of sample was blotted onto holey carbon grids previously glow discharged in a PELCO easiGlow discharger unit. Cryofrozen samples were held in a Leica EM GP cryo workstation to be finally observed in a JEM-2011 electron microscope (JEOL, Tokyo, Japan) operating at 200 kV. Temperature was always maintained at −180°C by continuous micro-additions of liquid ethane. Pictures were taken using a CCD-multiscan camera (Gatan, Pleasanton, CA).

DLS

Size distribution of small particles was characterized by DLS using a Zetasizer Nano ZS Instrument (Malvern Instruments, Malvern, UK) with a He/Ne 633 nm laser at 173°C. The hydrodynamic diameter and polydispersity index measurements were taken at 25°C and 0.8872 cP. Samples were manually plunged into disposable 1 mL cuvettes (Scharlab, Barcelona, Spain). Data collection consisted in 16 scans resulting in a mean value. Also, each sample was automatically measured three times to assess the measurement error of the device.

Western blot analysis

Samples were loaded and separated on SDS-PAGE and transferred onto a polyvinylidene difluoride membrane for 7 min using the system Trans-Blot Turbo Transfer System (Bio-Rad, Hercules, CA) properly following the manufacturer's guide. Membranes were incubated O/N with each corresponding primary antibody in 5% (w/v) non-fat dry milk 1× TBS 0.1% Tween 20 at 4°C with gentle shaking. Primary antibodies were as described: anti-TSG101 antibody (1:1,000, BD Biosciences, 612696), anti-actin antibody (1:2,000, Abcam, ab179467), anti-ALIX antibody (1:1,000, Abcam, ab275377), anti-CD9 antibody (1:2,000, Abcam, ab236630), anti-CD81 antibody (1:1,000, Abcam, ab79559), anti-CD63 antibody (1:1,000, Abcam, ab134045). Secondary incubation was performed with either anti-rabbit IgG or anti-mouse IgG bonded to alkaline phosphatase (provided by IBB, UAB, Barcelona, Spain) at RT for 1 h. Final membrane incubation with Clarity Western ECL substrates (Bio-Rad) allowed the chemiluminescence protein band to be revealed when exposed in a ChemiDoc MP (Bio-Rad).

Proteomic analysis

A proteomic identification study was carried out with the retentate sample coming from AEX chromatography by the Cardiovascular Proteomics group (CNIC, Madrid, Spain). Proteins were digested using sequencing-grade trypsin (Promega, Madison, WI) and the filter-assisted sample preparation technology (Expedeon, San Diego, CA). The resulting peptides were subjected to LC-MS/MS analysis on a nano-HPLC Easy nLC 1000 liquid chromatograph (Thermo Scientific) coupled to a QExactive mass spectrometer (Thermo Scientific). Protein identification was performed over the raw files using the SEQUEST HT algorithm integrated in the Proteome Discoverer 2.1 (Thermo Finnigan). Identified proteins were functionally annotated using the Gene Ontology database for both molecular function and biological process.[69,70] HEK293 secretome analysis was curated using the STRING database to form gene clusters, which were further edited using Cytoscape software.[71,72]

Infection of HEK293 cell cultures

Serotype 5 AdV E1AΔ-GFP was kindly provided by VCN Biosciences (Sant Cugat, Barcelona, Spain). AdV stocks were diluted with sterile-filtered PBS to infect cells at a multiplicity of infection of 10 at 1×10^6, 2×10^6, and 12×10^6 cell/mL. Appropriate MR was performed under the specified conditions, moments before infection, to ensure maximal removal of molecules contained in supernatants. Transfection with UGCG enzyme was performed 4 h prior to infection using standard transfection conditions described above.

AdV titer quantification

Samples were lysed using 10× lysis buffer (Tris-HCl 500 mM [T1503, Sigma-Aldrich], Triton X-100 1% [v/v] [9002-93-1, Sigma-Aldrich], $MgCl_2$ 20 mM [SLBP3227V, Sigma-Aldrich] [pH 7.5]) for 1 h at 37°C with gentle agitation. Lysed samples were kept at −80°C for storage. For the determination of vg titer; first, DNase I was added to lysed samples at 0.165 mg/mL (10104159001, Roche) and incubated at 37°C for 16 h in a DNase buffer (5 mM $CaCl_2$, 5 mM $MgCl_2$, 50 mM Tris-HCl [pH 8.0]). EDTA 30 mM (AM9260G, Invitrogen) was then added to each tube at and incubated at 70°C for 30 min to inactivate DNase I. Then, Proteinase K (2 mg/mL, EO0491, Thermo Fisher Scientific) was added and incubated at 55°C for 2 h and inactivated at 95°C, 15 min. qPCR reaction was set up using a set of primers specific to a region within the eGFP gene using an iTaq Universal SYBR Green Supermix (Bio-Rad) and the recommended thermocycling profile in a CFX384 Touch Real-Time PCR Detection System.

Data management and statistical analyses

Graphs were plotted using GraphPad Prism v.9.0.0. (San Diego, CA). Statistical differences were calculated in the same software with one-way ANOVA (Tukey test for multiple comparison) and 95% confidence. All experiments were run by three independent biological replicates. Microscopy image treatment, and diameter and density calculations, were performed with Fiji ImageJ[73] (SciJava, Open Source). 3D deconvolutions of confocal microscopy images were carried out using Imaris Software[74] (Oxford Instruments, Abingdon-on-Thames, UK).

DATA AND CODE AVAILABILITY

The data supporting the finding of this study can be found in the main text or the supplemental information. Additional information may be made available upon reasonable request to the corresponding author.

SUPPLEMENTAL INFORMATION

Supplemental information can be found online at https://doi.org/10.1016/j.omtm.2024.101190.

ACKNOWLEDGMENTS

This research was supported by grant PID2022-139019OB-I00 (Plan General del Conocimiento, Ministerio de Ciencia e Innovación, Gobierno de España). The research group Enginyeria de Bioprocessos i Biocatàlisi Aplicada ENG4BIO is recognized as 2021 SGR 00143 by Departament de Recerca i Universitats de la Generalitat de Catalunya. The authors would like to thank Dr. Amine Kamen (McGill University, Montreal, Canada) for providing the HEK293SF-3F6 cells and Dr. Ernest Milián Gonzalez (VCN Biosciences, Sant Cugat, Spain) for his generous contribution with the adenoviral stocks and qPCR validations. Technical help from Marc García Trujillo is highly appreciated. Support from José Amable Bernabé from the Institute of Material Science of Barcelona (ICMAB-CSIC, Barcelona Spain) with particle tracking techniques and the help of Martí de Cabo and Dr. Meritxell Vendrell from the Microscopy Service from the Universitat Autònoma de Barcelona (Barcelona, Spain) in the performance of electron and confocal microscopy analysis are very much appreciated. The authors would also like to show their gratitude to Inmaculada Jorge and Jesús Vázquez for the proteomic identification carried out at Centro Nacional de Investigaciones Cardiovasculares (CNIC, Madrid, Spain).

AUTHOR CONTRIBUTIONS

Conceptualization, P.P.-R. and J.L.-G.; experimentation, P.P.-R., J.L.-G., L.B.-M., and E.L.R.; investigation, P.P.-R. and J.L.-G.; writing – original draft, P.P.-R. and J.L.-G.; writing – review & editing. P.P.-R., J.L.-G., L.C., and F.G. Both co-first authors have agreed to list their names first in their CV.

DECLARATION OF INTERESTS

The authors declare no competing interests.

REFERENCES

1. Excler, J.L., Saville, M., Berkley, S., and Kim, J.H. (2021). Vaccine development for emerging infectious diseases. Nat. Med. *27*, 591–600.
2. Smith, J., Lipsitch, M., and Almond, J.W. (2011). Vaccine production, distribution, access, and uptake. Lancet *378*, 428–438.
3. Rajendra, Y., Hougland, M.D., Alam, R., Morehead, T.A., and Barnard, G.C. (2015). A high cell density transient transfection system for therapeutic protein expression based on a CHO GS-knockout cell line: Process development and product quality assessment. Biotechnol. Bioeng. *112*, 977–986.
4. Stuible, M., Burlacu, A., Perret, S., Brochu, D., Paul-Roc, B., Baardsnes, J., Loignon, M., Grazzini, E., and Durocher, Y. (2018). Optimization of a high-cell-density polyethylenimine transfection method for rapid protein production in CHO-EBNA1 cells. J. Biotechnol. *281*, 39–47.
5. Lai, T., Yang, Y., and Ng, S.K. (2013). Advances in mammalian cell line development technologies for recombinant protein production. Pharmaceuticals *6*, 579–603.
6. Baldi, L., Hacker, D.L., Adam, M., and Wurm, F.M. (2007). Recombinant protein production by large-scale transient gene expression in mammalian cells: State of the art and future perspectives. Biotechnol. Lett. *29*, 677–684.
7. Gutiérrez-Granados, S., Cervera, L., Kamen, A.A., and Gòdia, F. (2018). Advancements in mammalian cell transient gene expression (TGE) technology for accelerated production of biologics. Crit. Rev. Biotechnol. *38*, 918–940.
8. Pham, P.L., Kamen, A., and Durocher, Y. (2006). Large-scale transfection of mammalian cells for the fast production of recombinant protein. Mol. Biotechnol. *34*, 225–237.
9. Stuible, M., van Lier, F., Croughan, M.S., and Durocher, Y. (2018). Beyond preclinical research: production of CHO-derived biotherapeutics for toxicology and early-phase trials by transient gene expression or stable pools. Curr. Opin. Chem. Eng. *22*, 145–151.
10. Kimura, T., Ferran, B., Tsukahara, Y., Shang, Q., Desai, S., Fedoce, A., Pimentel, D.R., Luptak, I., Adachi, T., Ido, Y., et al. (2019). Production of adeno-associated virus vectors for in vitro and in vivo applications. Sci. Rep. *9*, 13601–13613.
11. Wright, J.F. (2009). Transient transfection methods for clinical adeno-associated viral vector production. Hum. Gene Ther. *20*, 698–706.
12. Bernal, V., Carinhas, N., Yokomizo, A.Y., Carrondo, M.J.T., and Alves, P.M. (2009). Cell density effect in the baculovirus-insect cells system: A quantitative analysis of energetic metabolism. Biotechnol. Bioeng. *104*, 162–180.
13. Dill, V., Ehret, J., Zimmer, A., Beer, M., and Eschbaumer, M. (2019). Cell density effects in different cell culture media and their impact on the propagation of foot-and-mouth disease virus. Viruses *11*, 511.
14. Mercille, S., Johnson, M., Lanthier, S., Kamen, A.A., and Massie, B. (2000). Understanding factors that limit the productivity of suspension-based perfusion cultures operated at high medium renewal rates. Biotechnol. Bioeng. *67*, 435–450.
15. Zeng, A.P. (1996). Quantitative assessment of cell density effect on the metabolism and antibody production rate of hybridoma cells at high cell density. J. Biotechnol. *45*, 243–251.
16. Huynh, H.T., Tran, T.T.B., Chan, L.C.L., Nielsen, L.K., and Reid, S. (2015). Effect of the peak cell density of recombinant AcMNPV-infected Hi5 cells on baculovirus yields. Appl. Microbiol. Biotechnol. *99*, 1687–1700.
17. Wu, Y., Bissinger, T., Genzel, Y., Liu, X., Reichl, U., and Tan, W.S. (2021). High cell density perfusion process for high yield of influenza A virus production using MDCK suspension cells. Appl. Microbiol. Biotechnol. *105*, 1421–1434.
18. Genzel, Y., Vogel, T., Buck, J., Behrendt, I., Ramirez, D.V., Schiedner, G., Jordan, I., and Reichl, U. (2014). High cell density cultivations by alternating tangential flow (ATF) perfusion for influenza A virus production using suspension cells. Vaccine *32*, 2770–2781.
19. Vázquez-Ramírez, D., Genzel, Y., Jordan, I., Sandig, V., and Reichl, U. (2018). High-cell-density cultivations to increase MVA virus production. Vaccine *36*, 3124–3133.
20. Lavado-García, J., Pérez-Rubio, P., Cervera, L., and Gòdia, F. (2022). The cell density effect in animal cell-based bioprocessing: Questions, insights and perspectives. Biotechnol. Adv. *60*, 108017.
21. Henry, O., Dormond, E., Perrier, M., and Kamen, A. (2004). Insights into adenoviral vector production kinetics in acoustic filter-based perfusion cultures. Biotechnol. Bioeng. *86*, 765–774.
22. Henry, O., Perrier, M., and Kamen, A. (2005). Metabolic flux analysis of HEK-293 cells in perfusion cultures for the production of adenoviral vectors. Metab. Eng. *7*, 467–476.
23. Cervera, L., Fuenmayor, J., González-Domínguez, I., Gutiérrez-Granados, S., Segura, M.M., and Gòdia, F. (2015). Selection and optimization of transfection enhancer additives for increased virus-like particle production in HEK293 suspension cell cultures. Appl. Microbiol. Biotechnol. *99*, 9935–9949.
24. Lavado-García, J., Jorge, I., Cervera, L., Vázquez, J., and Gòdia, F. (2020). Multiplexed Quantitative Proteomic Analysis of HEK293 Provides Insights into Molecular Changes Associated with the Cell Density Effect, Transient Transfection, and Virus-Like Particle Production. J. Proteome Res. *19*, 1085–1099.

25. Lavado-García, J., González-Domínguez, I., Cervera, L., Jorge, I., Vázquez, J., and Gòdia, F. (2020). Molecular Characterization of the Coproduced Extracellular Vesicles in HEK293 during Virus-Like Particle Production. J. Proteome Res. *19*, 4516–4532.

26. Doyle, L.M., and Wang, M.Z. (2019). Overview of Extracellular Vesicles, Their Origin, Composition, Purpose, and Methods for Exosome Isolation and Analysis. Cells *8*, 727.

27. Van Niel, G., D'Angelo, G., and Raposo, G. (2018). Shedding light on the cell biology of extracellular vesicles. Nat. Rev. Mol. Cell Biol. *19*, 213–228.

28. Yáñez-Mó, M., Siljander, P.R.M., Andreu, Z., Zavec, A.B., Borràs, F.E., Buzas, E.I., Buzas, K., Casal, E., Cappello, F., Carvalho, J., et al. (2015). Biological properties of extracellular vesicles and their physiological functions. J. Extracell. Vesicles *4*, 27066–27160.

29. Vlassov, A.V., Magdaleno, S., Setterquist, R., and Conrad, R. (2012). Exosomes: Current knowledge of their composition, biological functions, and diagnostic and therapeutic potentials. Biochim. Biophys. Acta *1820*, 940–948.

30. Schiera, G., Di Liegro, C.M., and Di Liegro, I. (2015). Extracellular Membrane Vesicles as Vehicles for Brain Cell-to-Cell Interactions in Physiological as well as Pathological Conditions. BioMed Res. Int. *2015*, 152926.

31. Sung, B.H., Ketova, T., Hoshino, D., Zijlstra, A., and Weaver, A.M. (2015). Directional cell movement through tissues is controlled by exosome secretion. Nat. Commun. *6*, 7164.

32. Alexander, M., Hu, R., Runtsch, M.C., Kagele, D.A., Mosbruger, T.L., Tolmachova, T., Seabra, M.C., Round, J.L., Ward, D.M., and O'Connell, R.M. (2015). Exosome-delivered microRNAs modulate the inflammatory response to endotoxin. Nat. Commun. *6*, 7321.

33. Liu, Y., Gu, Y., Han, Y., Zhang, Q., Jiang, Z., Zhang, X., Huang, B., Xu, X., Zheng, J., and Cao, X. (2016). Tumor Exosomal RNAs Promote Lung Pre-metastatic Niche Formation by Activating Alveolar Epithelial TLR3 to Recruit Neutrophils. Cancer Cell *30*, 243–256.

34. Rilla, K., Mustonen, A.M., Arasu, U.T., Härkönen, K., Matilainen, J., and Nieminen, P. (2019). Extracellular vesicles are integral and functional components of the extracellular matrix. Matrix Biol. *75–76*, 201–219.

35. Lawson, C., Vicencio, J.M., Yellon, D.M., and Davidson, S.M. (2016). Microvesicles and exosomes: New players in metabolic and cardiovascular disease. J. Endocrinol. *228*, R57–R71.

36. Costa-Silva, B., Aiello, N.M., Ocean, A.J., Singh, S., Zhang, H., Thakur, B.K., Becker, A., Hoshino, A., Mark, M.T., Molina, H., et al. (2015). Pancreatic cancer exosomes initiate pre-metastatic niche formation in the liver. Nat. Cell Biol. *17*, 816–826.

37. Williams, C., Royo, F., Aizpurua-Olaizola, O., Pazos, R., Boons, G.J., Reichardt, N.C., and Falcon-Perez, J.M. (2018). Glycosylation of extracellular vesicles: current knowledge, tools and clinical perspectives. J. Extracell. Vesicles *7*, 1442985.

38. Colombo, M., Raposo, G., and Théry, C. (2014). Biogenesis, Secretion, and Intercellular Interactions of Exosomes and Other Extracellular Vesicles. Annu. Rev. Cell Dev. Biol. *30*, 255–289.

39. Mulcahy, L.A., Pink, R.C., and Carter, D.R.F. (2014). Routes and mechanisms of extracellular vesicle uptake. J. Extracell. Vesicles *3*.

40. Payne, C.K., Jones, S.A., Chen, C., and Zhuang, X. (2007). Internalization and trafficking of cell surface proteoglycans and proteoglycan-binding ligands. Traffic *8*, 389–401.

41. Hiraga, C., Yamamoto, S., Hashimoto, S., Kasahara, M., Minamisawa, T., Matsumura, S., Katakura, A., Yajima, Y., Nomura, T., and Shiba, K. (2021). Pentapartite fractionation of particles in oral fluids by differential centrifugation. Sci. Rep. *11*, 3326–3415.

42. Théry, C., Witwer, K.W., Aikawa, E., Alcaraz, M.J., Anderson, J.D., Andriantsitohaina, R., Antoniou, A., Arab, T., Archer, F., Atkin-Smith, G.K., et al. (2018). Minimal information for studies of extracellular vesicles 2018 (MISEV2018): a position statement of the International Society for Extracellular Vesicles and update of the MISEV2014 guidelines. J. Extracell. Vesicles *7*, 1535750.

43. Lavado-García, J., Díaz-Maneh, A., Canal-Paulí, N., Pérez-Rubio, P., Gòdia, F., and Cervera, L. (2021). Metabolic engineering of HEK293 cells to improve transient transfection and cell budding of HIV-1 virus-like particles. Biotechnol. Bioeng. *118*, 1649–1663.

44. Drews, K., Calgi, M.P., Harrison, W.C., Drews, C.M., Costa-Pinheiro, P., Shaw, J.J.P., Jobe, K.A., Han, J.D., Fox, T.E., White, J.M., and Kester, M. (2020). Glucosylceramide synthase maintains influenza virus entry and infection. PLoS One *15*, e0228735.

45. Das, A., Barrientos, R., Shiota, T., Madigan, V., Misumi, I., McKnight, K.L., Sun, L., Li, Z., Meganck, R.M., Li, Y., et al. (2020). Gangliosides are essential endosomal receptors for quasi-enveloped and naked hepatitis A virus. Nat. Microbiol. *5*, 1069–1078.

46. Drake, M.J., Brennan, B., Briley, K., Bart, S.M., Sherman, E., Szemiel, A.M., Minutillo, M., Bushman, F.D., and Bates, P. (2017). A role for glycolipid biosynthesis in severe fever with thrombocytopenia syndrome virus entry. PLoS Pathog. *13*, e1006316.

47. González-Domínguez, I., Grimaldi, N., Cervera, L., Ventosa, N., and Gòdia, F. (2019). Impact of physicochemical properties of DNA/PEI complexes on transient transfection of mammalian cells. N. Biotech. *49*, 88–97.

48. González-Domínguez, I., Puente-Massaguer, E., Lavado-García, J., Cervera, L., and Gòdia, F. (2022). Micrometric DNA/PEI polyplexes correlate with higher transient gene expression yields in HEK 293 cells. N. Biotech. *68*, 87–96.

49. Veziroglu, E.M., and Mias, G.I. (2020). Characterizing Extracellular Vesicles and Their Diverse RNA Contents. Front. Genet. *11*, 700–730.

50. Statello, L., Maugeri, M., Garre, E., Nawaz, M., Wahlgren, J., Papadimitriou, A., Lundqvist, C., Lindfors, L., Collén, A., Sunnerhagen, P., et al. (2018). Identification of RNA-binding proteins in exosomes capable of interacting with different types of RNA: RBP-facilitated transport of RNAs into exosomes. PLoS One *13*, e0195969.

51. de Maio, A. (2011). Extracellular heat shock proteins, cellular export vesicles, and the Stress Observation System: A form of communication during injury, infection, and cell damage: It is never known how far a controversial finding will go! Dedicated to Ferruccio Ritossa. Cell Stress Chaperones *16*, 235–249.

52. Willms, E., Cabañas, C., Mäger, I., Wood, M.J.A., and Vader, P. (2018). Extracellular vesicle heterogeneity: Subpopulations, isolation techniques, and diverse functions in cancer progression. Front. Immunol. *9*, 738.

53. Balasubramaniam, M., and Freed, E.O. (2011). New insights into HIV assembly and trafficking. Physiology *26*, 236–251.

54. Hessvik, N.P., and Llorente, A. (2018). Current knowledge on exosome biogenesis and release. Cell. Mol. Life Sci. *75*, 193–208.

55. Kavaliauskiene, S., Nymark, C.M., Bergan, J., Simm, R., Sylvänne, T., Simolin, H., Ekroos, K., Skotland, T., and Sandvig, K. (2014). Cell density-induced changes in lipid composition and intracellular trafficking. Cell. Mol. Life Sci. *71*, 1097–1116.

56. Sillence, D.J., Puri, V., Marks, D.L., Butters, T.D., Dwek, R.A., Pagano, R.E., and Platt, F.M. (2002). Glucosylceramide modulates membrane traffic along the endocytic pathway. J. Lipid Res. *43*, 1837–1845.

57. Tetta, C., Ghigo, E., Silengo, L., Deregibus, M.C., and Camussi, G. (2013). Extracellular vesicles as an emerging mechanism of cell-to-cell communication. Endocrine *44*, 11–19.

58. van Niel, G., Carter, D.R.F., Clayton, A., Lambert, D.W., Raposo, G., and Vader, P. (2022). Challenges and directions in studying cell–cell communication by extracellular vesicles. Nat. Rev. Mol. Cell Biol. *23*, 369–382.

59. Frantz, C., Stewart, K.M., and Weaver, V.M. (2010). The extracellular matrix at a glance. J. Cell Sci. *123*, 4195–4200.

60. Wessels, D.J., Pradhan, N., Park, Y.N., Klepitsch, M.A., Lusche, D.F., Daniels, K.J., Conway, K.D., Voss, E.R., Hegde, S.v., Conway, T.P., and Soll, D.R. (2019). Reciprocal signaling and direct physical interactions between fibroblasts and breast cancer cells in a 3D environment. PLoS One *14*, e0218854.

61. Kuriyama, N., Yoshioka, Y., Kikuchi, S., Azuma, N., and Ochiya, T. (2020). Extracellular Vesicles Are Key Regulators of Tumor Neovasculature. Front. Cell Dev. Biol. *8*, 611039–611116.

62. Becker, A., Thakur, B.K., Weiss, J.M., Kim, H.S., Peinado, H., and Lyden, D. (2016). Extracellular Vesicles in Cancer: Cell-to-Cell Mediators of Metastasis. Cancer Cell *30*, 836–848.

63. Nawaz, M., Shah, N., Zanetti, B.R., Maugeri, M., Silvestre, R.N., Fatima, F., Neder, L., and Valadi, H. (2018). Extracellular vesicles and matrix remodeling enzymes: The emerging roles in extracellular matrix remodeling, progression of diseases and tissue repair. Cells *7*, 167–226.

64. Dar, G.H., Mendes, C.C., Kuan, W.L., Speciale, A.A., Conceição, M., Görgens, A., Uliyakina, I., Lobo, M.J., Lim, W.F., el Andaloussi, S., et al. (2021). GAPDH controls

extracellular vesicle biogenesis and enhances the therapeutic potential of EV mediated siRNA delivery to the brain. Nat. Commun. *12*, 7357.

65. Schömel, N., Gruber, L., Alexopoulos, S.J., Trautmann, S., Olzomer, E.M., Byrne, F.L., Hoehn, K.L., Gurke, R., Thomas, D., Ferreirós, N., et al. (2020). UGCG overexpression leads to increased glycolysis and increased oxidative phosphorylation of breast cancer cells. Sci. Rep. *10*, 8182–8213.

66. Bielser, J.M., Wolf, M., Souquet, J., Broly, H., and Morbidelli, M. (2018). Perfusion mammalian cell culture for recombinant protein manufacturing – A critical review. Biotechnol. Adv. *36*, 1328–1340.

67. Lavado-García, J., Jorge, I., Boix-Besora, A., Vázquez, J., Gòdia, F., and Cervera, L. (2021). Characterization of HIV-1 virus-like particles and determination of Gag stoichiometry for different production platforms. Biotechnol. Bioeng. *118*, 2660–2675.

68. Cervera, L., González-Domínguez, I., Segura, M.M., and Gòdia, F. (2017). Intracellular characterization of Gag VLP production by transient transfection of HEK 293 cells. Biotechnol. Bioeng. *114*, 2507–2517.

69. Ashburner, M., Ball, C.A., Blake, J.A., Botstein, D., Butler, H., Cherry, J.M., Davis, A.P., Dolinski, K., Dwight, S.S., Eppig, J.T., et al. (2000). Gene Ontology : tool for the unification of biology. Nat. Genet. *25*, 25–29.

70. The Gene Ontology Consortium, Dietze, H., Lewis, S.E., Mungall, C.J., Munoz-Torres, M.C., Basu, S., Chisholm, R.L., Dodson, R.J., Fey, P., Thomas, P.D., et al. (2017). Expansion of the gene ontology knowledgebase and resources: The gene ontology consortium. Nucleic Acids Res. *45*, 331–338.

71. Szklarczyk, D., Gable, A.L., Nastou, K.C., Lyon, D., Kirsch, R., Pyysalo, S., Doncheva, N.T., Legeay, M., Fang, T., Bork, P., et al. (2021). The STRING database in 2021: Customizable protein-protein networks, and functional characterization of user-uploaded gene/measurement sets. Nucleic Acids Res. *49*, 605–612.

72. Shannon, P., Markiel, A., Ozier, O., Baliga, N.S., Wang, J.T., Ramage, D., Amin, N., Schwikowski, B., and Ideker, T. (2003). Cytoscape: A software Environment for integrated models of biomolecular interaction networks. Genome Res. *13*, 2498–2504.

73. Schneider, C.A., Rasband, W.S., and Eliceiri, K.W. (2012). NIH Image to ImageJ: 25 years of image analysis. Nat. Methods *9*, 671–675.

74. Haass-Koffler, C.L., Naeemuddin, M., and Bartlett, S.E. (2012). An analytical tool that quantifies cellular morphology changes from three-dimensional fluorescence images. J. Vis. Exp. *2*, e4233–e4236.